Research Square

Preprints are preliminary reports that have not undergone peer review.
They should not be considered conclusive, used to inform clinical practice,
or referenced by the media as validated information.

CS@UiO-66-NH_2@rGO hydrogel beads for synergistic adsorptive removal of tetracycline and norfloxacin in batch and continuous systems

Yue Li
University of Malaya
Si Yuan zhang
University of Malaya
Ping Xiang
Southwest Forestry University
Chin Wei Lai
cwlai@um.edu.my
University of Malaya
Chia Jing Chang
University of Malaya

Research Article

Keywords: UiO-66-NH_2, In situ synthesis, Antibiotic, Adsorption

Posted Date: June 22nd, 2026

DOI: https://doi.org/10.21203/rs.3.rs-9891550/v1

License: This work is licensed under a Creative Commons Attribution 4.0 International License.
Read Full License

Additional Declarations: No competing interests reported.

CS@UiO-66-NH_2@rGO hydrogel beads for synergistic adsorptive removal of tetracycline and norfloxacin in batch and continuous systems

Yue Li [a, b], Si Yuan Zhang [a], Ping Xiang [d], Chin Wei Lai [a, c]*, Chia Jing Chang [a, c]*

[a] Institute for Advanced Studies (IAS), Universiti Malaya, Kuala Lumpur 50603, Malaysia

[b] Institute of Art and Design, Huaihua University, Huaihua 418000, China

[c] Nanotechnology and Catalysis Research Centre (NANOCAT), Universiti Malaya, Kuala Lumpur 50603, Malaysia

[d] Institute of Environmental Remediation and Human Health, School of Ecology and Environment, Southwest Forestry University, Kunming 650224, China

* **Corresponding author**:

Prof. Dr. Chin Wei Lai (cwlai@um.edu.my)

Dr. Chia Jing Chang (rickychia2u@gmail.com).

Address: University of Malaya, Institute for Advanced Studies, Advanced Studies Complex, 50603 Kuala Lumpur, Federal Territory of Kuala Lumpur

Abstract: We developed a novel composite hydrogel bead (CS@UiO-66-NH_2@rGO) by promoting the in situ crystallization and stabilization of UiO-66-NH_2 within a dual-network framework composed of chitosan (CS) and reduced graphene oxide (rGO). The developed adsorbent exhibits pronounced affinity toward norfloxacin (NOR) and tetracycline (TC), enabling simultaneous and high-capacity uptake under both mono-component and coexisting pollutant conditions. Batch adsorption results revealed that the prepared beads maintained outstanding removal capability across a wide pH spectrum, with maximum adsorption efficiency observed under mildly acidic conditions. Langmuir isotherm analysis yielded monolayer adsorption capacities (q_m) of 511.78 $mg \cdot g^{-1}$ for TC and 320.67 $mg \cdot g^{-1}$ for NOR. The adsorption behavior of both antibiotics was more accurately described by the pseudo-second-order (PSO) kinetic equation and the Langmuir model, as evidenced by the superior correlation coefficients obtained from data fitting. The adsorption mechanism can therefore be attributed predominantly to chemisorptive interactions occurring at energetically homogeneous active sites, consistent with a monolayer adsorption pattern. Even after undergoing five consecutive regeneration cycles, the material preserved most of its removal efficiency, demonstrating remarkable structural stability and reusability. Under binary conditions, the hydrogel beads achieved removal efficiencies of 92.5% for TC and 82.8% for NOR at pH 6.5, demonstrating their pronounced synergistic performance in treating mixed contaminant systems. In addition, in a simulated fixed-bed continuous-flow system suitable for practical application, when the breakthrough point ($C = 1\ mg \cdot L^{-1}$) was used as the criterion, the cumulative treated volumes reached 420 mL for TC and 380 mL

for NOR, respectively, indicating a stable potential for continuous treatment. Comprehensive structural and surface analyses suggest that TC and NOR uptake is driven by multiple interactive pathways, including occupation of internal pore domains, aromatic π-electron interactions, hydrogen-bond formation, and metal–ligand coordination involving Zr active centers.

Keywords: UiO-66-NH_2；In situ synthesis；Antibiotic；Adsorption

1. Introduction

NOR and TC have been extensively applied in human medicine and livestock production owing to their high therapeutic efficacy, relatively low toxicity, and broad-spectrum activity (Gaballah et al., 2023; Gaspari et al., 2024; Kweon et al., 2025). However, the absorption efficiency of antibiotics in animals is generally low, and approximately 70–90% of the administered dose is excreted as parent compounds or active metabolites, which constitutes a significant source of antibiotic contamination in the environment (Haenni et al., 2022; Larsson & Flach, 2022). Recent monitoring studies have detected NOR and TC in livestock and poultry manure from Austria, China, Germany, Belgium, and other countries (Frey et al., 2022; F. Guo et al., 2025; Ram & Kumar, 2020; Treskova et al., 2022). They are global environmental contaminants. The pollutants reach the soil and water medium mainly through the application of manures as fertilizers, and the run-off during rains makes microbes resistant to antibiotics, upsets the ecological balance, and may even pose serious environmental and public health risks such as the development of `superbugs' (Adebisi, 2023; Serwecińska, 2020).

Rapid approaches with high efficiency are needed to tackle the problem of the persistence of antibiotic residues in terrestrial and aquatic ecosystems (Zhaomeng Wu et al., 2025).

In the past few decades, there have been studies on various material systems with different physicochemical properties that help treat antibiotics (de Ilurdoz et al., 2022; Samrot et al., 2023). Among the treatment technologies, adsorption shows great potential in antibiotic removal owing to its operational simplicity, low energy consumption, non-generation of secondary by-products, and relative ease of engineering application (Deng et al., 2025; Stylianou et al., 2021).The functional materials are designed on various structural platforms by altering the mechanism of interaction with fluoroquinolone and tetracycline contaminants (D. Liu et al., 2023; F. Zhang et al., 2023; X. Zheng et al., 2024). However, the high affinity of most of these functionalized materials is determined by contaminants, say either fluoroquinolone or tetracycline. Even though some reports have shown that iron-based trimetallic metal–organic frameworks (MOFs) can simultaneously remove TC and NOR from water, the development of high-performance adsorbents capable of 'dual-function removal with a single material' is seldom seen (Noori Keshtkar et al., 2025; Wei et al., 2023). This has significantly limited their practical application in the case of combined pollution scenarios (Gao et al., 2024). In this context, bead-type adsorbents not only enhance material operability and separability but also improve adsorption stability over a wide pH range, offering superior environmental adaptability compared with photocatalytic materials, which typically exhibit high efficiency only under neutral conditions

(Abdullah et al., 2025). Meanwhile, modified biochar materials generally show limited adsorption capacity toward TC (L. Zhang et al., 2025). Overall, the development of an efficient, acid-alkali-resistant, easily separable, and bifunctional composite bead adsorbent is of critical importance for the synergistic remediation of antibiotic co-contamination and provides new insights into the design of green and high-efficiency pollution control materials (Chai et al., 2022).

MOFs have attracted considerable attention in environmental pollution control owing to their tunable structures and high porosity (Cai et al., 2021). Among them, UiO-66-NH_2 has emerged as a representative MOF due to its excellent water stability, making it particularly suitable for the adsorption of aqueous pollutants (Sun, 2025). Due to their adjustable coordination architectures and abundant internal void space, MOFs offer many active sites and structural flexibility, making them excellent materials for removing diverse organic pollutants (He et al., 2021; N. Li et al., 2024). Some studies have reported MOFs with high antibiotic adsorption, such as UiO-66-NH_2, which has an adsorption capacity for NOR in water of up to 222.5 $mg \cdot g^{-1}$ (H.-M. Zhang et al., 2024). However, powder MOFs have several inherent disadvantages, including small particle size, easy dispersion, difficult recovery, and secondary pollution, which severely limit their engineering applications (Cheng et al., 2020; R. Li et al., 2023). The embedding of MOFs into a CS matrix overcomes these drawbacks and yields composite beads with excellent mechanical strength, easy separation, recyclability, and environmental compatibility (Abdalkarim et al., 2025).

CS is a biopolymer that is abundantly available in nature, highly biocompatible, and biodegradable (Sathiyaseelan et al., 2025). Because of its green properties and low cost, it has been widely used in the preparation of adsorbent materials. It is particularly suitable for use as a supporting matrix for composite beads (Musarurwa & Tavengwa, 2022a). Various studies have shown that CS-based aerogels and hydrogels have good performance properties for the removal of antibiotics (Bento et al., 2025; Q. Liu et al., 2025).For instance, ZIF-67 hydrogel beads were prepared, showing a maximum adsorption capacity of 94.71 mg g^{-1} for ofloxacin and TC, indicating good potential for fluoroquinolone removal (H. Yang et al., 2024). The hydrogel network can quickly swell in aqueous solution and provide a large number of active functional groups, thereby improving the binding capacity for pollutants (Weerasundara et al., 2021); however, over-swelling can significantly reduce mechanical strength, especially in natural biopolymer matrices (Calderon Moreno et al., 2025). To overcome this problem, graphene materials have recently been used because of their excellent self-gelation properties (Xiong et al., 2020). The addition of rGO can significantly improve the anti-swelling behavior and mechanical strength of hydrogels, enabling their application in continuous-flow systems, such as fixed beds, and thereby expanding their engineering applicability (Yue et al., 2023). Moreover, the rich oxygen-containing functional groups on the surface of rGO can provide hydrogen bonding and π–π stacking interactions, thereby markedly enhancing the adsorption capacity for antibiotics containing aromatic rings (Carrales-Alvarado et al., 2020; Yao et al., 2020). Therefore, the addition of rGO into the CS matrix can greatly improve the structural rigidity of the biopolymer matrix

while also creating a strong three-dimensional scaffold that can provide controlled nucleation and uniform crystallization of UiO-66-NH_2 in the hydrogel matrix (Y. Guo et al., 2025; Mi et al., 2025).

The objectives of this research were to synthesize CS@UiO-66-NH_2@rGO composite beads for efficient removal of NOR and TC and to comprehensively investigate their application potential in single-solute, coexisting-solute, and continuous-flow systems. The objectives were as follows: (1) to evaluate the influence of solution acidity, starting dosage, thermal conditions, and simultaneous inorganic ions on the adsorption performance; (2) to explore the rate-controlling steps, site occupation, and energy variation trends by fitting kinetic, isotherm, and thermodynamic models; (3) to use multiscale characterization methods to compare the differences in material structure and surface chemical environments before and after adsorption, and to explore the adsorption mechanism; (4) to investigate the synergistic adsorption capacity and competitive effects in NOR-TC coexisting systems; (5) to investigate the stability and dynamic removal capacity of the beads as fixed-bed packing materials in continuous-flow systems; and (6) to comprehensively investigate reusability and feasibility by conducting cyclic regeneration experiments.

2. Materials and methods

CS, characterized by a deacetylation level exceeding 95% and a viscosity range of 100–200 mPa·s, glacial acetic acid, ethanol, and NOR ($C_{16}H_{18}FN_3O_3$, ≥98%) were purchased from Adamas. The reagents employed included TC ($C_{22}H_{24}N_2O_8$, purity ≥98%), $ZrCl_4$ (purity ≥99%), anhydrous DMF, and H_2BDC-NH_2 (≥98%), which were utilized as the

metal precursor and organic linker for MOF synthesis, and rGO (>99%) was obtained from Aladdin. The solution pH was regulated using dilute HCl and NaOH solutions. To simulate ionic interference, NaCl and $CaCl_2$ were introduced as background electrolytes for the preparation of competing ion systems. Methanol, ethanol, and acetonitrile were utilized in desorption and regeneration experiments. Nitrogen gas (N_2, ≥99.999%) was used for Brunauer–Emmett–Teller (BET) analysis, and potassium bromide (KBr) was used for Fourier transform infrared (FTIR) pellet preparation. High-purity water with a specific resistance of 18.2 MΩ·cm was used to prepare all liquid samples. Stock solutions of NOR and TC (1000 $mg \cdot L^{-1}$) were prepared in advance, stored in amber bottles at 4 °C in the dark, and diluted to the desired working concentrations before use (H. Yang et al., 2024). All reagents were used as received, according to the specified grades, without further purification unless otherwise stated.

2.2. Preparation of CS, CS@UiO-66-NH_2, and CS@UiO-66-NH_2@rGO

In this study, composite beads were prepared using a "bead formation and solidification followed by solvothermal in situ growth" strategy. At the outset, 70 mL of 1% (w/v) acetic acid was used as the solvent, into which 1.50 g of CS was gradually added under constant magnetic stirring until a homogeneous, transparent solution was obtained. Subsequently, 2.33 g of $ZrCl_4$ was added to the system and stirred constantly to ensure complete incorporation into the polymer matrix. Meanwhile, 30 mg of rGO was dispersed in 30 mL of deionized water and ultrasonicated for 30 minutes to form a stable suspension, which was then added dropwise to the CS-$ZrCl_4$ solution with mechanical stirring until a uniform precursor solution was formed. The precursor solution was then

slowly added to 300 mL of 1.0 M NaOH solution under continuous stirring, at which point rapid gelation occurred, forming spherical beads. At the same time, Zr^4+ ions underwent hydrolysis and precipitation due to the alkaline environment, forming $Zr(OH)_4$, which was then immobilized in the CS matrix to form the CS@$Zr(OH)_4$@rGO composite intermediate beads. After completion of the dropwise addition, stirring was continued at room temperature for 5 hours to allow for solidification and stabilization of the structure, followed by thorough washing with deionized water until the eluate was neutralized.

For comparison purposes, two control samples were also synthesized: (1) CS beads, which were synthesized under the same conditions but without the addition of $ZrCl_4$ and rGO; and (2) $Zr(OH)_4$-coated CS beads ($Zr(OH)_4$@CS), which were synthesized under the same conditions but without rGO. Subsequently, the Zr(OH)4@CS and CS beads were separately soaked in 60 mL of N, N-dimethylformamide (DMF) solution containing 1.82 g of 2-aminoterephthalic acid (H2BDC-NH2), and the mixture was allowed to stand at 100 °C for 24 h to facilitate the nucleation and crystallization of UiO-66-NH_2 on the surface of the beads. After the reaction, the beads were washed three times with deionized water to remove any unreacted ligands and solvent. Finally, the beads were freeze-dried to retain their porous structure. For ease of discussion in the following sections, the synthesized samples are referred to as CS, CS@UiO-66-NH_2, and CS@UiO-66-NH_2@rGO.

2.3. Structural analysis

The microstructural features and surface characteristics of the prepared composites were characterized using a Nano SEM-450 instrument (FEI, USA), enabling detailed observation of their morphology as well as assessment of elemental dispersion and compositional features. FTIR (Vertex70; Bruker, Germany) was employed to identify functional groups in the CS@UiO-66-NH_2@rGO composite; measurements were performed using the KBr pellet method, in which sample powders were mixed with KBr at a mass ratio of 1:100 (m/m) and scanned over the wavenumber range of 4000–400 cm^{-1}. The crystalline phases of the composite beads were examined by XRD (D8 ADVANCE A25, Bruker, Germany). Diffraction patterns were collected within a 2θ interval of 5°–60°, operated at 40 kV with a tube current of 30 mA. Textural properties of the samples, including surface area and porosity characteristics, were evaluated by recording nitrogen sorption isotherms at 77 K on a Quantachrome Autosorb IQ-SN instrument (USA) and analyzing the data using the BET model. The surface chemical environment and elemental distribution of the samples, both before and after adsorption, were investigated using a PHI VersaProbe 3 XPS system (USA). All binding energy values were referenced to the C 1s peak at 284.8 eV for calibration. Thermal behavior was examined using TGA (STA7200RV, HITACHI, Japan) under nitrogen, with a heating rate of 20 ℃·min^{-1} to assess the stability of the composite materials.

2.4. Evaluation of adsorption performance

2.4.1. Evaluation of adsorption under batch conditions

For the batch studies, concentrated mother solutions of NOR and TC were first prepared at 1000 mg·L^{-1}, then diluted to obtain the required starting concentrations. All batch

tests were conducted in a thermostatic air-bath shaker (THZ-82A; Kexing, China) at 160 rpm for 24 h. The solution pH was adjusted using 0.01 $mol \cdot L^{-1}$ NaOH or 0.01 $mol \cdot L^{-1}$ HCl. For single-component systems, the concentrations of NOR and TC were monitored at their respective maximum absorption wavelengths with a UV–Vis instrument (UV1902, Shanghai Aoyi Scientific Instrument). In contrast, high-performance liquid chromatography (HPLC) was employed for binary NOR–TC solutions to avoid interference caused by overlapping spectra. All adsorption experiments, except those designed for thermodynamic evaluation, were conducted at 303 K.

The adsorption behavior of CS@UiO-66-NH_2@rGO beads was evaluated under varying operational conditions, including solution pH, contact duration, initial pollutant concentration, temperature, and the presence of competing species (Nguyen et al., 2024). To investigate pH effects, adsorption experiments were performed using a 30 mL antibiotic solution containing 15 mg of adsorbent, with pH regulated over 3–12 (Yu et al., 2025). Kinetic experiments were conducted by sampling at predetermined time intervals from 0 to 24h to monitor variations in NOR/TC concentrations. Isotherm analyses were performed over initial concentrations ranging from 30 to 1000 $mg \cdot L^{-1}$, and temperatures of 293 K, 303 K, and 313 K. To simulate real-world aqueous conditions, the effect of co-present cations (Na^+, K^+, Ca^{2+}, Mg^{2+}), anions (Cl^-, NO_3^-, SO_4^{2-}), and organic solvents (methanol, ethanol, acetonitrile) on adsorption capacity was investigated. For the desorption analysis, saturated adsorption beads were shaken with methanol, ethanol, and acetonitrile for 6 hours to identify the best eluent, and

ethanol showed the highest desorption efficiency. It was selected as the regenerant for five consecutive adsorption-desorption cycles.

To evaluate the potential of the CS@UiO-66-NH_2@rGO composite beads for continuous-flow applications, dynamic adsorption studies were conducted in a fixed-bed column. A cylindrical glass reactor with an internal diameter of 15 mm and a height of 100 mm was filled with 100 mg of CS@UiO-66-NH_2@rGO hydrogel beads. At room temperature (308 K), antibiotic solutions with an initial concentration of 20 $mg \cdot L^{-1}$ (NOR or TC) were continuously fed downward through the fixed-bed column at a constant flow rate of 1.25 $mL \cdot min^{-1}$ using a peristaltic pump (Lead Fluid BT300L, China). Periodic effluent sampling was conducted throughout the experiment, and the collected data were subsequently processed to generate breakthrough profiles.

2.5 Data processing procedures

All experiments were conducted in triplicate. The removal efficiency (R%) and the adsorption capacities at any given time and at equilibrium, qt and qe ($mg \cdot g^{-1}$), respectively, were calculated using the following equations (Viltres et al., 2024) (Equations (1)–(3)).

$$R(\%) = \frac{C_0 - C_t}{C_0} \quad (1)$$

$$q_e = \frac{(C_0 - C_e) \times V}{m} \quad (2)$$

$$\boldsymbol{q_t} = \frac{(C_0 - C_t) \times V}{m} \quad (3)$$

In the adsorption calculations, C_0, C_t, and C_e ($mg \cdot L^{-1}$) are defined as the NOR concentrations measured at the beginning of the experiment, at a specific contact time,

and after equilibrium was reached, respectively. The symbol m denotes the amount of oven-dried adsorbent employed (mg), while V denotes the total solution volume used in each batch system (mL).

For the fixed-bed experiments, the volume of treated effluent (V_{eff}) was determined in accordance with Eq. (4); Equation (5) was employed to quantify the cumulative uptake (mg) under a defined influent velocity condition; and Equation (6) was utilized to evaluate the overall adsorptive loading normalized to the adsorbent mass (q_e, $mg \cdot g^{-1}$) upon completion of the dynamic flow experiment.

$$V_{eff} = Q t_{total} \tag{4}$$

$$q_{total} = \frac{Q}{1000} \int_{t=0}^{t=t_{total}} C_{ad} dt \tag{5}$$

$$q_{eq} = \frac{q_{total}}{w} \tag{6}$$

In this expression, t_{total} corresponds to the overall operational duration (min), whereas Q represents the volumetric feed rate expressed in $mL \cdot min^{-1}$. The total adsorption capacity during dynamic adsorption is calculated from the area under the breakthrough curve obtained by integrating the adsorption concentration (C_{ad}; $mg \cdot L^{-1}$) with respect to time (min), where w represents the mass of the adsorbent (g).

3. Results and discussion

3.1. Structural and morphological analysis

As shown in Scheme 1, the CS@UiO-66-NH_2@rGO composite beads were successfully prepared. Microscopy observations revealed that the synthesized hydrogel beads exhibited consistent sphericity, with a mean size measuring approximately 2 mm.

The UiO-66-NH_2 component imparted a light yellow color to the beads, while the addition of rGO led to a gradual shift in color from light yellow to dark gray. To confirm the structural arrangement and surface characteristics of the materials prior to the adsorption experiment, a series of physicochemical analyses was conducted.

The specimens were examined via a scanning electron microscope (SEM) to investigate their physical features. The pristine CS beads had a smooth, spherical morphology with a homogeneous surface and no surface defects (Fig. 1A). However, the CS beads loaded with UiO-66-NH_2 (CS@UiO-66-NH_2) (Fig. 1B) had a highly roughened surface with numerous porous sites, suggesting that the metal-organic framework significantly increased the surface roughness and porosity. After the loading of rGO, the CS@UiO-66-NH_2@rGO beads had a highly wrinkled surface with significantly increased surface roughness (Fig. 1C).

FTIR spectroscopy (Fig. 2A) was used to analyze the functional groups present in UiO-66-NH_2 powder. The broad absorption peak at 3400 cm^{-1} was attributed to the stretching vibrations of –NH_2/–OH groups (Shirazian et al., 2025). The band at 1660 cm^{-1} was ascribed to the C=O stretching vibration, while the band at 1580 cm^{-1} was assigned to the –NH_2 bending and aromatic C=C stretching vibrations (Kang et al., 2025). The absorption peak at 1390 cm^{-1} was due to the C–N stretching vibration, while the peak at 675 cm^{-1} was assigned to the Zr–O framework vibrations (Yousaf et al., 2026). The CS beads had a broad –OH/–NH_2 band at 3400 cm^{-1}, a –CH_2– stretching vibration at 2900 cm^{-1}, an amide I band at 1660 cm^{-1}, and a characteristic C–O–C vibration of

glycosidic bonds at 1060 cm^{-1}, thus confirming its polysaccharide origin (Guo et al., 2026).

The CS@UiO-66-NH_2 hybrid material retained the principal characteristic peaks of CS. It exhibited more pronounced absorption bands at 1580 cm^{-1}, 1390 cm^{-1}, and 675 cm^{-1}, corresponding to –NH_2/C=C, C–N, and Zr–O vibrations of UiO-66-NH_2, respectively, indicating that the MOF was successfully constructed and stably embedded within the CS matrix (Zehao Li et al., 2021). In the CS@UiO-66-NH_2@rGO composite, the aromatic C=C/–NH_2 band near 1580 cm^{-1} became further intensified and slightly broadened, which was attributed to the π-conjugated structures introduced by rGO sheets, confirming the effective incorporation of rGO into the composite (Vinesh et al., 2020). Overall, the synergistic introduction of UiO-66-NH_2 and rGO significantly altered the chemical structure and functional-group environment of the material, confirming the successful construction of the ternary composite and its potential for adsorption (Ma et al., 2025).

Furthermore, after treatment of CS@UiO-66-NH_2@rGO under pH = 3 and pH = 12 conditions, the positions and intensities of the prominent characteristic FTIR peaks remained essentially unchanged (Fig. S1), indicating excellent chemical stability and structural integrity of the composite and supporting its long-term applicability in complex aqueous environments (Bouaziz et al., 2023).

As shown in Fig. 2B, the XRD spectrum of the CS@UiO-66-NH_2@rGO composite exhibits characteristic peaks at about 7.4°, 8.6°, 12.1°, 14.9°, and 16.6°. These values are similar to those of the XRD spectrum of UiO-66-NH_2 MOF and correspond to the

(111), (200), (220), (311), and (222) reflections of the fcu structure, respectively, as reported in the literature (Fang et al., 2020). This implies the successful formation of the UiO-66-NH_2 MOF in the CS/rGO matrix (Tai et al., 2025). Compared to the XRD spectrum of the pure UiO-66-NH_2, the XRD spectrum of the composite has the same peak values, and there are no impurity peaks, suggesting that the formation of the composite did not affect the crystalline structure of the MOF (Z. Li et al., 2023). In addition, there are no characteristic peaks corresponding to the CS and rGO, which could be due to the amorphous nature of the two materials (Ge et al., 2020).

The textural properties of CS, CS@UiO-66-NH_2, and CS@UiO-66-NH_2@rGO were characterized by BET analysis (Fig. 2C). The specific surface area was found to be 17.45 $m^2 \cdot g^{-1}$ for CS, indicating a limited number of accessible micro/mesoporous sites (Balakrishnan et al., 2023). However, upon loading UiO-66-NH_2 onto CS, the specific surface area increased significantly to 165.89 $m^2 \cdot g^{-1}$, indicating that MOF loading significantly increased the number of accessible adsorption sites (Mojtahedi et al., 2025). The mean pore diameter was 3.12 nm for CS@UiO-66-NH_2, indicating a mesoporous framework (Liang et al., 2023). Upon loading rGO onto CS@UiO-66-NH_2, the specific surface area was found to increase to 298.76 $m^2 \cdot g^{-1}$, and measurements indicated an average pore size of 3 nm. This indicates that loading rGO onto CS@UiO-66-NH_2 improved the textural properties and facilitated the adsorption (More et al., 2023). This evolution in the structure provides a larger number of adsorption sites and better mass transfer for the subsequent adsorption of TC and NOR (Chen et al., 2021).

TGA of CS@UiO-66-NH_2@rGO has shown a three-step weight loss profile for the composite material, as depicted in Fig. 2D. It has been observed that the weight loss of the composite material is low in the low-temperature range of 30 to 150°C. The weight loss of 3.17% is attributed to the removal of water molecules adsorbed on the composite material (Moaty et al., 2025). The weight loss of the composite material is significant in the range of 150-450/500°C. The 48.14% weight loss is due to CS degradation in the composite material. This weight loss is consistent with the degradation of organic compounds in the composite material (C. Wang et al., 2020). In the high-temperature region (approximately 500–700 ℃), a further gradual weight loss of ~5.91% was observed, attributable to continued decomposition or carbonization of residual carbonaceous species and the transformation toward more stable inorganic phases (Z. Zhao et al., 2026). Above 700 ℃, the mass stabilized, with a final residue of approximately 40–45%, indicating a relatively high proportion of inorganic residues, which are expected to consist predominantly of Zr-based inorganic phases with minor carbonaceous remnants (Rr & Haimbodi, 2026).

3.2. Adsorptive behavior of antibiotics in single-solute systems

3.2.1. Performance comparison of different adsorbent materials

Batch adsorption systems were established by introducing 0.015 g of each material (CS, rGO, UiO-66-NH_2, CS@UiO-66-NH_2, and CS@UiO-66-NH_2@rGO) into 30 mL of TC or NOR aqueous solutions prepared at an initial concentration of 50 $mg \cdot L^{-1}$ for comparative evaluation, and the adsorption trials were carried out at a controlled temperature of 303 K. As shown in Fig. 3A and 3B, all materials exhibited similar trends

in adsorption capacity for NOR and TC. Pristine CS beads showed relatively low adsorption capacities for NOR (22.45 $mg \cdot g^{-1}$) and TC (22.16 $mg \cdot g^{-1}$), primarily due to their small specific surface area, limited porosity, and the low number of accessible active sites (C. Liu et al., 2020). In contrast, rGO exhibited moderately enhanced adsorption capacities for NOR (31.78 $mg \cdot g^{-1}$) and TC (32.15 $mg \cdot g^{-1}$), which can be attributed to its higher specific surface area and the presence of additional π–π interaction sites arising from its aromatic sheet structure (Shahabi et al., 2024).

UiO-66-NH_2 powder exhibited further increased adsorption capacities for NOR (65.34 $mg \cdot g^{-1}$) and TC (64.27 $mg \cdot g^{-1}$). Its well-defined porous framework and amino-functionalized ligands provide abundant coordination, hydrogen-bonding, and electrostatic-interaction sites for both antibiotics (Badri et al., 2025). However, the powder form is prone to aggregation and exhibits limited dispersibility in aqueous media, which hinders the full utilization of active sites. Upon uniform immobilization of UiO-66-NH_2 within the CS matrix, CS@UiO-66-NH_2 displayed significantly improved adsorption capacities for NOR (75.92 $mg \cdot g^{-1}$) and TC (76.15 $mg \cdot g^{-1}$) (J. Li et al., 2024). The CS matrix promotes the dispersion and stabilization of UiO-66-NH_2 microcrystals, alleviates aggregation in solution, and simultaneously enhances mechanical integrity and recyclability (Hu et al., 2022).

With the further incorporation of rGO, CS@UiO-66-NH_2@rGO achieved the highest adsorption capacities for NOR (80.53 $mg \cdot g^{-1}$) and TC (81.59 $mg \cdot g^{-1}$). This enhancement reflects a pronounced synergistic effect among the hydrophilic porous network of CS, the highly porous framework of UiO-66-NH_2, and the π-conjugated

sheet structure of rGO in the ternary composite (Zou et al., 2021). On the one hand, this synergy increases the specific surface area and mesopore fraction of the composite, mitigates MOF aggregation, and improves structural stability (Lingxia Lu et al., 2022); on the other hand, it effectively reduces mass-transfer resistance and facilitates the diffusion and multipoint adsorption of NOR and TC molecules, thereby substantially enhancing the overall removal performance for both antibiotics (Abdelfatah et al., 2022; Hao et al., 2021).

3.2.2. Effects of pH and coexisting ions

Considering that CS tends to swell or dissolve under strongly acidic conditions (Keshvardoostchokami et al., 2021). In contrast, its adsorption capacity is markedly reduced under strongly alkaline conditions, the adsorption behavior of CS@UiO-66-NH_2@rGO composite beads toward NOR and TC was systematically investigated over a pH range of 3–12 (Fig. 3C). As shown, the removal efficiencies of both antibiotics exhibited a similar pH-dependent trend, initially increasing and subsequently decreasing, with maximum values observed under weakly acidic conditions. Within the examined pH range (3–6), a pronounced enhancement in adsorption performance was observed. The NOR removal rate increased from 52.4% to 92.8%, while the TC removal rate increased from 45.6% to 95.8%. When the pH increased from 6 to 7, both removal efficiencies remained above 90% but showed a slight decline from their peak values at pH 6. At pH $\geq$ 8, the removal efficiencies decreased markedly, with a more pronounced decline observed in the alkaline region (pH 9–12).

This pH-dependent behavior is closely associated with the coupled effects of solution pH on the adsorbent's surface charge and the speciation of the antibiotic molecules (Musarurwa & Tavengwa, 2022b). The ΔpH–pH_0 curve indicates that the point of zero charge (pH_{pzc}) of the composite is approximately 7.8 (Fig. 3D). Below pH 7.8, the adsorbent exhibits a net positive surface charge. In contrast, it becomes progressively negatively charged at pH > 7.8. NOR exhibits two pK_a values (pK_{a1} = 6.22 and pK_{a2} = 8.51); it exists mainly as a cation (NOR^+) at pH < 6.2, as a neutral species (NOR^0) in the pH range of 6.2–8.5, and increasingly as an anion (NOR^-) at pH > 8.5 (Djidja et al., 2025). Therefore, at the optimal pH of approximately 6, NOR is present predominantly in a neutral or near-neutral form, while the adsorbent surface remains slightly positively charged (B. Wang et al., 2023). Within this experimental setup, electrostatic repulsion is minimal, enabling NOR molecules to more readily access the pores of UiO-66-NH_2 and be effectively adsorbed through hydrogen bonding, π–π stacking, and interactions with Zr sites (Y. Zhang et al., 2025).

TC contains multiple dissociable functional groups (typical pK_a ≈ values 3.3, 7.7, and 9.7) and predominantly exists in a zwitterionic or near-neutral form over the pH range 3.3–7.7. Accordingly, under pH 6–7 conditions, TC can also be efficiently captured through multipoint hydrogen bonding, π–π interactions, and coordination or complexation with Zr nodes (Y. Zhao et al., 2025). When pH > 8, both NOR and TC increasingly exist in anionic forms, while the adsorbent surface becomes more negatively charged, leading to enhanced electrostatic repulsion (X. Liu et al., 2024; Xu et al., 2025). Simultaneously, deprotonation of –NH_2 groups on CS and UiO-66-NH_2

weakens hydrogen-bonding interactions, and increased competition from OH^- ions and hydration effects further attenuates hydrophobic and π–π interactions, collectively resulting in a pronounced decrease in removal efficiency (Jansen et al., 2022; Jin et al., 2026).

3.2.4. Kinetic analysis of the adsorption process

To investigate the time-dependent adsorption dynamics of TC and NOR, batch tests using CS@UiO-66-NH_2@rGO beads were conducted for up to 24 h (Luo et al., 2024). The corresponding adsorption profiles are presented in Fig. 4A and 4B. Both antibiotics exhibited a pronounced rapid adsorption stage at the initial period, indicating that a large number of readily accessible active sites were available on the bead surface and within the hierarchical pore structure (C. Zheng et al., 2024). Within the first 5 h, the TC removal efficiency increased rapidly, reaching approximately 85%, corresponding to an adsorption capacity of about 85 $mg \cdot g^{-1}$. Similarly, NOR exhibited rapid uptake within the first 4 h, with removal efficiency exceeding 85% and an adsorption capacity of about 86 $mg \cdot g^{-1}$.

As the contact time increases, the number of available adsorption sites on the surface of composite beads becomes progressively occupied, resulting in a significant decrease in the uptake rate and a gradual approach to equilibrium in the adsorption performance of TC and NOR, characterized by a stable uptake state (Sutherland, 2025). As the active sites become saturated, the system approaches adsorption equilibrium, and any further increase in adsorption capacity becomes negligible. The following mathematical

expressions can describe the adsorption kinetics (Alamgir et al., 2020), and the corresponding kinetic parameters are summarized in Table 1.

Specifically, the process was interpreted according to the pseudo-first-order (PFO) formulation:

$$\ln(q_e - q_t) = \ln q_e - K_1 t \quad (7)$$

The PSOkinetics model：

$$\frac{t}{q_t} = \frac{1}{q_e{}^2 K_2} + \frac{t}{q_e} \quad (8)$$

The parameters q_e and q_t ($mg \cdot g^{-1}$) are defined as the amounts of adsorbate retained per unit mass of adsorbent at equilibrium and at any selected contact time t, respectively. The kinetic parameters k_1 (h^{-1}) and k_2 ($g \cdot mg^{-1} \cdot h^{-1}$) correspond to the rate coefficients associated with the PFO and PSO models (Ezzati, 2024).

Comparative fitting results indicated that the adsorption behavior aligned more closely with the PSO kinetic expression than with the first-order model, supported by near-unity R^2 values for both TC and NOR. In addition, the q_e values predicted by the PSO equation showed substantial conformity with the experimental data, suggesting that this kinetic model provides a more reliable representation of TC and NOR uptake on the CS@UiO-66-NH_2@rGO surface (Ezzati, 2024). Based on the PSO kinetic fitting, the calculated k_2 values were 0.0444 $g \cdot mg^{-1} \cdot h^{-1}$ (TC) and 0.04812 $g \cdot mg^{-1} \cdot h^{-1}$ (NOR) (Mukherjee et al., 2023). These results indicate that chemical interactions play a dominant role in controlling the adsorption kinetics of both antibiotics (J. Wang & Guo, 2020).

3.2.5. Adsorption isotherms

The equilibrium adsorption data for NOR and TC were fitted to the Langmuir and the Freundlich isotherm models to determine the maximum adsorption capacities of the material and elucidate the adsorption characteristics and interfacial interactions governing the adsorption process (Lei Lu & Na, 2022). The corresponding mathematical expressions are given as follows:

Langmuir adsorption model — monolayer uptake on energetically uniform sites:

$$\frac{C_e}{q_e} = \frac{1}{q_m K_L} + \frac{C_e}{q_m} \quad (9)$$

Freundlich model describing non-uniform surface energy distribution and multilayer adsorption behavior:

$$\ln\ q_e = \frac{1}{n} \ln\ C_e + \ln\ K_F \quad (10)$$

In the isotherm equations, q_m ($mg \cdot g^{-1}$) corresponds to the theoretical monolayer uptake capacity. In contrast, K_L ($L \cdot mg^{-1}$) and K_F are associated with the affinity parameters of the Langmuir and the Freundlich models. The exponent n characterizes adsorption intensity, and values of n greater than unity indicate a favorable adsorption process (Tran et al., 2021).

The Langmuir and the Freundlich fitting curves for TC and NOR at different temperatures are presented in Fig. 4C and 4D, respectively.. The fitting results indicate that the Langmuir equation provides better agreement with the experimental data than the Freundlich model, suggesting that monolayer adsorption on homogeneous active sites predominates in this system. This finding suggests that the adsorption of TC and NOR on the CS@UiO-66-NH_2@rGO surface proceeds via a monolayer-saturation mechanism at relatively homogeneous adsorption sites (Alnajrani & Alsager, 2020). Langmuir isotherm fitting revealed monolayer adsorption capacities (q_m) of 511.78 $mg \cdot g^{-1}$ for TC and 320.67 $mg \cdot g^{-1}$ for NOR. Compared with other reported adsorbents (Table 2), CS@UiO-66-NH_2@rGO exhibits superior adsorption performance and outperforms most analogous materials documented in the literature.

3.2.6. Thermodynamic analysis

Thermodynamic parameters were derived from adsorption isotherms obtained at different temperatures to assess the temperature responsiveness of TC and NOR uptake. The relevant thermodynamic parameters were calculated using Equations (11)–(13), and the results are summarized in Table 3.

$$\Delta G = -RT\ln\ \mathrm{K_0} \tag{11}$$

$$\ln\ \mathrm{K_0} = \frac{\Delta \mathrm{S}}{\mathrm{R}} - \frac{\Delta \mathrm{H}}{\mathrm{RT}} \tag{12}$$

$$\mathrm{K_0} = 10^6 \times \mathrm{K_L} \tag{13}$$

Herein, R is the universal gas constant (8.314 $J \cdot mol^{-1} \cdot K^{-1}$); K_L ($L \cdot mol^{-1}$) represents the Langmuir isotherm constant; and ΔG, ΔH, and ΔS correspond to the Gibbs free energy ($kJ \cdot mol^{-1}$), enthalpy ($kJ \cdot mol^{-1}$), and entropy ($kJ \cdot mol^{-1}$), respectively (H. Wang et al., 2021).

As the temperature increased from 293 to 313 K, the adsorption capacities of TC and NOR on CS@UiO-66-NH_2@rGO increased, and the Langmuir constants increased with increasing temperature, indicating that the adsorption process is favored at higher temperatures (Imanipoor et al., 2021). Within the applied temperature range, the Gibbs free energy change (ΔG) for the adsorption of the two antibiotics was negative (-22.77 to -25.90 kJ/mol), and the values increased with increasing temperatur. This indicates that the adsorption process is spontaneous, and it is favored at higher temperatures (Fig. 4C, D)(Sallam et al., 2023).

As indicated in Table 3 above, the enthalpy changes (ΔH) related to the adsorption of TC and NOR by the adsorbent material CS@UiO-66-NH2@rGO are positive, thus supporting the endothermic nature of the adsorption process by this adsorbent material(Bi et al., 2022). The positive ΔH value related to the adsorption of NOR (22.88

kJ/mol) suggests that aside from the role of physical and chemical interactions in the adsorption process, there is an equally important role played by other interactions in the adsorption mechanism (Khan et al., 2021). In contrast, the lower ΔH value for TC adsorption by the adsorbent indicates that, in this adsorption mechanism, physical interactions are more prominent role (L. Yang et al., 2024). Moreover, the positive entropy changes (ΔS) related to the adsorption of the two antibiotics by the adsorbent material indicate an increase in disorder in the interface of the adsorbent and the solution (R. Zhao et al., 2021). This is usually attributed to the displacement of water molecules in the solution as the adsorbent material adsorbs the antibiotics (Xia et al., 2021).

3.2.7. Effects of coexisting ions

In a real wastewater treatment process, various inorganic ions and organic species are commonly present, and their effects on the adsorption efficiency of pollutants cannot be ignored, as they may interfere with adsorption through charge screening, competitive adsorption, and complexation (Gan et al., 2024). To examine the effects of coexisting species on the adsorption behavior of antibiotics by the CS@UiO-66-NH_2@rGO composite beads, this study has investigated the effects of typical monovalent and divalent inorganic cations such as Na^+, K^+, Ca^{2+}, and Mg^{2+}, common inorganic anions such as Cl^-, NO_3^-, and SO_4^{2-} (Fig. 5B), and various organic solvents such as methanol, ethanol, and acetonitrile (Fig. 5A). The obtained data clearly indicate that monovalent cations (Na^+ and K^+) and monovalent anions (Cl^- and NO_3^-) exerted negligible effects on the removal efficiencies of both antibiotics. The system maintained relatively high

adsorption performance. This observation indicates that the adsorption process does not rely solely on electrostatic interactions but is primarily governed by the synergistic contributions of hydrogen bonding, π–π interactions, and coordination between antibiotic molecules and Zr nodes (Isaeva et al., 2021). In contrast, divalent cations Ca^{2+} and Mg^{2+} exhibited more pronounced inhibitory effects on adsorption, with Ca^{2+} causing the most potent suppression (Yongjia et al., 2024). This behavior is likely attributable to its stronger charge-screening ability and higher coordination affinity, which promote competitive binding with surface functional groups such as $–NH_2$ and –OH on the adsorbent, thereby reducing the number of available active sites (Ali et al., 2025). Moreover, Ca^{2+} may modify the surface microenvironment through complexation or "bridging effects," further weakening the effective interactions between the adsorbent and TC or NOR (Abou-Elyazed et al., 2024). Because TC contains multiple functional groups capable of complexation or coordination, its removal efficiency decreases more in the presence of divalent cations Evaluation of tetracycline removal by magnetic metal organic framework from aqueous solutions: Adsorption isotherm, kinetics, thermodynamics, and Box-Behnken design optimization (Abumelha et al., 2023).

Apparent differences in the inhibitory effects among anions were found. Compared to $Cl^–$ and $NO_3^–$, a more pronounced inhibitory effect of $SO_4^{2–}$ on TC and NOR adsorption could be related to its higher charge density and higher hydration capability (Obeso et al., 2024). The inhibitory effects of coexisting organic solvents on TC and NOR adsorption were also evaluated. It was found that methanol, ethanol, and acetonitrile

inhibited TC and NOR adsorption to varying degrees, while maintaining high adsorption capacities. Among these solvents, ethanol had the least inhibitory effect, while acetonitrile had the most potent inhibitory effect on TC and NOR adsorption. This could be related to the change in solvent polarity induced by these solvents and their effects on the solvation status of TC and NOR molecules, resulting in a decrease in hydrogen bonding and hydrophobic interaction between TC/NOR molecules and the adsorbent surface, as well as π-π stacking interaction and mass transfer within the adsorbent particles (S. Tang et al., 2024). It can be concluded that the CS@UiO-66-NH_2@rGO composite beads have good resistance to monovalent ions and certain organic solvents. However, a higher inhibitory effect of Ca^{2+} and a higher charge density anion on TC/NOR adsorption could be related to their higher inhibitory effects on TC/NOR adsorption (Hooriabad Saboor et al., 2022; A. L. T. Zheng et al., 2025). This indicates that water hardness and ionic composition should be taken into account when this material is used in a complex water environment (Bhattacharyya et al., 2021; Dutta & Mala, 2020).

3.2.8. Adsorption–desorption cycles

The reusability of adsorbents is crucial for assessing their economic viability in wastewater treatment (Bathula et al., 2025). It was found that, compared to adsorbents in powder form, CS-based hydrogel beads can be easily recovered by filtration after adsorption (Tao et al., 2023). Therefore, the separation of adsorbents can be significantly simplified, thereby reducing the risk of secondary pollution (Selvam et al., 2023). The recyclability of CS@UiO-66-NH_2@rGO was assessed. The highest

regeneration efficiency was achieved with ethanol, which was then used to regenerate the adsorbent in the subsequent adsorption/desorption tests. The regeneration efficiency of CS@UiO-66-NH_2@rGO was assessed by using five consecutive adsorption/desorption tests (Fig. 5C). It is noted that, after several cycles of regeneration, the adsorption capacity of TC and NOR showed a trend of gradual decrease. However, the attenuation of the adsorption capacity is not significant. To be specific, the removal efficiency of TC decreased from 93.8% in the first cycle to 78.3% in the fifth cycle, while that of NOR decreased from 90.9% to 76.8%. The gradual decrease in removal performance can be ascribed to the retention of antibiotic molecules in internal pores or at strong adsorption sites, which are not fully desorbable during regeneration (Khezerlou et al., 2025). However, the CS@UiO-66-NH_2@rGO material presents a stable framework and regeneration ability during the repeated adsorption/desorption tests, indicating its potential for use in engineering applications (Aguila-Rosas et al., 2025).

3.2.9 Column experiments

In order to test the suitability of CS@UiO-66-NH_2@rGO in a dynamic system, a laboratory-scale column setup was designed, taking advantage of the excellent sorption potential of the sorbent as well as the spherical shape of the sorbent particles (Quan & Zhang, 2024). The setup was designed to mimic a continuous sorption process for the removal of TC and NOR in water. The schematic representation of the setup, along with the breakthrough curves, is shown in Fig. 6A. During the dynamic test, the initial solution concentration was maintained at 20 $mg \cdot L^{-1}$, and the flow rate was 1.25

$mL \cdot min^{-1}$. The lab was found to have the potential to completely remove TC and NOR in the initial stage, as indicated by the absence of contaminants in the solution (Abdi & Abedini, 2020). This suggests the availability of sufficient sorption sites in the column as well as the presence of unimpeded mass transfer sites (Abdi & Abedini, 2020).

With more extended periods of operation, it was observed that the effluent concentration increased gradually, finally reaching the breakthrough point at which C = 1 $mg \cdot L^{-1}$. Also, the breakthrough curve for NOR occurred earlier than that for TC, indicating that the fixed bed was breached by NOR before it was by TC (Yi Zhou et al., 2022). Upon reaching a breakthrough, the cumulative treated volumes for TC and NOR reached 420 mL and 380 mL, respectively, demonstrating that the dynamic removal capacity of the fixed bed for TC is slightly higher than that for NOR. Based on integration of the breakthrough curves using Equation (5), the area under the breakthrough curves for TC and NOR were 5672.0 $mg \cdot min \cdot L^{-1}$ and 4974.4 $mg \cdot min \cdot L^{-1}$, respectively. Breakthrough analysis indicated that the column achieved dynamic uptake values (q_{column}) of 70.90 $mg \cdot g^{-1}$ for TC and 62.18 $mg \cdot g^{-1}$ for NOR, which are slightly lower than the equilibrium adsorption capacities (q_e) obtained from batch experiments at the same initial concentration (20 $mg \cdot L^{-1}$). This discrepancy is primarily attributed to limited contact time and intrabed mass-transfer resistance during fixed-bed operation (Hosono & Uemura, 2021).

The column experiments were conducted at room temperature (308 K). In conjunction with the thermodynamic analysis, the adsorption of both TC and NOR is endothermic, and moderate increases in temperature favor increased adsorption capacity. In contrast,

dynamic adsorption under continuous-flow conditions is more strongly constrained by residence time and mass-transfer processes (Zhanming Li et al., 2022). Overall, CS@UiO-66-NH_2@rGO composite beads exhibit favorable removal performance and stable breakthrough behavior for both TC and NOR during continuous fixed-bed operation, demonstrating substantial potential for practical water treatment engineering applications (Hou et al., 2020).

3.3. Adsorption performance of TC and NOR in a binary system

In batch adsorption conditions, the adsorption behavior of CS@UiO-66-NH2@rGO beads for the binary tetracycline and norfloxacin (TC-NOR) system was investigated. This investigation simulated the presence of multiple antibiotics in the wastewater (Gai et al., 2020). he results show that the beads removed the two antibiotics simultaneously with high efficiency under mild acidic conditions (pH ~ 6.5) (Fig. 6C). When the two components were tested individually, the TC and NOR adsorption efficiencies were 90.2% and 83.2%, respectively. However, in the binary system, the TC adsorption efficiency remained high at 80.6%, indicating minimal competitive influence and a strong adsorption preference. However, NOR efficiency decreased significantly to 65.3%, indicating a clear disadvantage for NOR. This could be due to the molecular structure of TC, which has a high number of hydroxyl, amide, and aromatic functional groups (Zhang et al., 2021). This allows TC to occupy high-energy adsorption sites with greater affinity, thereby reducing the number of effective adsorption sites for NOR through competitive exclusion (K. Wang et al., 2020). However, the beads still show a

high efficiency for the simultaneous adsorption of the two antibiotics under batch conditions (C.-Y. Wang et al., 2022).

To assess the engineering feasibility of the CS@UiO-66-NH_2@rGO beads, a fixed-bed continuous system was implemented to investigate the adsorbent's removal performance for TC/NOR in a dynamic system. As presented in Fig. 6D, the mean elimination efficiencies of TC/NOR in the dynamic single-solute system were observed to be 78.5%/68.2%, respectively. Compared with the adsorbent's equilibrium adsorption capacity in the static system, the efficiencies decreased slightly. This can be attributed to the shorter contact times of the solutes with the adsorbent material in the fixed-bed system (F. Zhang et al., 2025). When the system was changed to a dynamic binary system, the effect of the competing solutes became more pronounced. In the binary system, the average removal efficiency of TC was observed to be 69.4%, while the average removal efficiency of NOR was observed to be only 50.5%. This significant difference in the removal efficiencies of the two solutes indicates the presence of a "competitive displacement" effect during the fixed-bed continuous system (Aziz et al., 2025). This effect can be defined as the preferential adsorption of the solute with the stronger affinity onto the adsorbent material, leading to the earlier breakthrough of the less-adsorbed solute from the fixed bed (Sporsho et al., 2025).

3.4. Adsorption mechanism

The adsorption mechanisms need to be elucidated to understand the basis of the material’s performance and its potential application in engineering practice (Ahmadijokani et al., 2024). Adsorption mechanisms can be physical adsorption and

chemical adsorption (Fakhraei Ghazvini et al., 2021). In the present study, the mechanisms of adsorption of TC and NOR by the composite material CS@UiO-66-NH_2@rGO were systematically investigated using a combination of BET, FTIR, and XPS techniques. Initially, the specific surface area and porosity of the material provide the fundamental basis of adsorption (Ghaedi et al., 2025). Prior to adsorption, the composite material has a specific surface area of 312.7 $m^2 \cdot g^{-1}$. It has a hierarchical porous structure. After adsorption of TC and NOR, the specific surface area of the composite material drastically decreases to 96.4 $m^2 \cdot g^{-1}$ and 68.9 $m^2 \cdot g^{-1}$ (Table S1). In addition, the pore volume decreases to 0.21 $cm^3 \cdot g^{-1}$ and 0.17 $cm^3 \cdot g^{-1}$. Concurrently, only a small fraction of the larger mesopores is preserved in the pore size distribution. In the case of TC adsorption, D is approximately 28.6 nm. For of NOR adsorption, the value of D is approximately 41.3 nm. This indicates that the antibiotic molecules penetrate the composite material's pores (M. Zheng et al., 2025). Consequently, the composite material's porosity decreases drastically (Ha et al., 2025). This indicates that the hierarchical porous structure of the composite material plays an important role in preserving mass transfer and enriching adsorbate molecules (Abbas et al., 2025). This indicates that the antibiotic molecules adsorb to the composite material via physical adsorption. This indicates that the adsorption of the antibiotic molecules by the composite material can be described as adsorption within the material's pores (Miao et al., 2022).

Combined with the kinetic and isotherm fitting results, the adsorption behaviors of TC and NOR can be more accurately described by the PSO kinetic model and the Langmuir

isotherm model, suggesting that the adsorption process involves both surface site occupation and electronic or chemical interactions and is dominated by monolayer saturation adsorption (Kaur et al., 2023). This implies that, in addition to pore volume filling, chemical interactions between surface functional groups and metal nodes are crucial for adsorption performance (Teng et al., 2025). To further clarify the microscopic mechanisms of interaction, comparative FTIR and XPS analyses before and after adsorption can provide direct evidence. In the FTIR spectra (Fig. 6B), the –OH/–NH stretching vibration band exhibits a pronounced red shift from approximately 3362 cm^{-1} to 3285–3288 cm^{-1}, accompanied by band broadening, indicating the formation of stronger hydrogen-bonding networks between surface –OH/–NH_2 groups and hydroxyl, carbonyl/amide, and nitrogen-containing functionalities in TC and NOR molecules (Z. Liu et al., 2021). In addition, because both TC and NOR contain aromatic ring structures, the π-electron systems provided by rGO sheets and the organic ligands of UiO-66-NH_2 can interact with these molecules through π–π stacking, thereby promoting molecular enrichment and stable binding at the surface and pore entrances (Ma et al., 2025).

XPS results further corroborate the involvement of chemical interactions. In the survey spectrum (Fig. 7A), a distinct F 1s signal appears after NOR adsorption, directly confirming the successful loading of NOR on the composite surface (Zixuan Wu et al., 2022). XPS curve fitting of the C 1s region (Fig. 7B) reveals distinct contributions attributed to C–C/C=C (~284.8 eV), C–N (~285.8–286.3 eV), C–O (~286.5 eV), and O–C=O/C=O species (~288–289 eV). Post-adsorption, changes in peak positions and

intensities are due to alterations in the electronic environment of carbon-containing functional groups upon the addition of antibiotics (Lin et al., 2023). In the N 1s spectrum of the sample, as shown in Figure 7C, there is a slight shift in the peaks corresponding to the C-N/C=N bond, indicating that the interaction between the $–NH_2$ group and antibiotic molecules is stronger upon adsorption (Farahbakhsh et al., 2025). Moreover, in the Zr 3d spectrum of the sample, as shown in Figure 7D, there is no significant change in the peak positions of the Zr 3d5/2 and Zr 3d3/2 double peaks, indicating that the structure of the Zr-O node in the UiO-66-NH_2 framework is not significantly changed upon adsorption. At the same time, the Lewis acid sites of Zr may be involved in the coordination of the carbonyl, hydroxyl, or nitrogen-containing groups of TC and NOR, leading to the enhancement of immobilization capacity (Sultana et al., 2025).

In summary, the adsorption of TC and NOR by the CS@UiO-66-NH_2@rGO adsorbent can be ascribed to the synergistic interplay of multiple adsorption mechanisms. In particular, the hierarchical porous structure and increased specific surface area provide the adsorbent with sufficient adsorption capacity through the pores, while the hydrogen bonding effect of $–NH_2$/–OH groups, π-π stacking effect of rGO and organic ligands, and Zr node-coordination effect can be regarded as the main chemical adsorption mechanisms (Fig. 8) (Istirokhatun et al., 2025).

4. Conclusion

The current study describes the fabrication of CS@UiO-66-NH_2@rGO composite hydrogel beads for the removal of antibiotics such as TC and NOR from aqueous

systems. The composite hydrogel beads have a high surface area, high structural stability, high efficiency over a pH range of 6.5, minimal impact from common ions, and high adsorption capacities of 511.78 mg/g for TC and 320.67 mg/g for NOR, which are much higher than those of other conventional adsorbents. Thermodynamic evaluation unequivocally establishes that the adsorption process is spontaneous ($\Delta G < 0$) and intrinsically endothermic ($\Delta H > 0$), with elevated temperatures further promoting sorption from an energetic standpoint. Thermodynamic analysis shows that the adsorption is spontaneous ($\Delta G < 0$) and endothermic ($\Delta H > 0$), with higher temperatures promoting sorption. Regeneration and fixed-bed tests indicate that the composite beads retain high removal efficiency and stable breakthrough performance during repeated cycles and continuous operation. The adsorption of NOR and TC is driven by pore-filling, hydrogen bonding, π–π interactions, and coordination to Zr active sites. Overall, the CS@UiO-66-NH_2@rGO beads exhibit good stability and reusability for the removal of mixed antibiotics, warranting further long-term testing in real wastewater systems.

Acknowledgments

The present work was funded by the Ministry of Higher Education，Malaysia for niche area research under the Higher institution Centre of Excellence (HICoE) program （JPT(BKPI)1000/016/018/28 JId.3(2) & NANOCAT-2024D）， the National Natural Science Foundation of China (42367064), and the Yunnan Thousand Youth Talent Program (YNQR-QNRC-2018-049).

Authorship contribution statement

Conceptualization, Chin Wei Lai; Methodology, Yue Li, Si Yuan Zhang, Ping Xiang, Chia Jing Chang; Software, Yue Li, Si Yuan Zhang, Chia Jing Chang; Validation, Chia Jing Chang; Formal Analysis, Yue Li; Data Curation, Si Yuan Zhang, Ping Xiang; Writing – Original Draft Preparation, Yue Li; Writing – Review & Editing, Chin Wei Lai; Supervision, Chin Wei Lai; Project Administration, Yue Li; Funding Acquisition, Ping Xiang, Chin Wei Lai.

Table captions

Table 1. Kinetic behavior of TC and NOR over CS@UiO-66-NH_2@rGO composite beads.

Antibiotics	Pseudo-first-order			Pseudo-second-order		
	qe (mg · g−1)	K1 (h−1)	R2	qe (mg · g−1)	K2 (g · mg−1 · h−1)	R2
TC	91.48	2.17	0.9788	95.24	0.0444	0.9946
NOR	92.182	2.35	0.9829	95.18	0.04812	0.9989

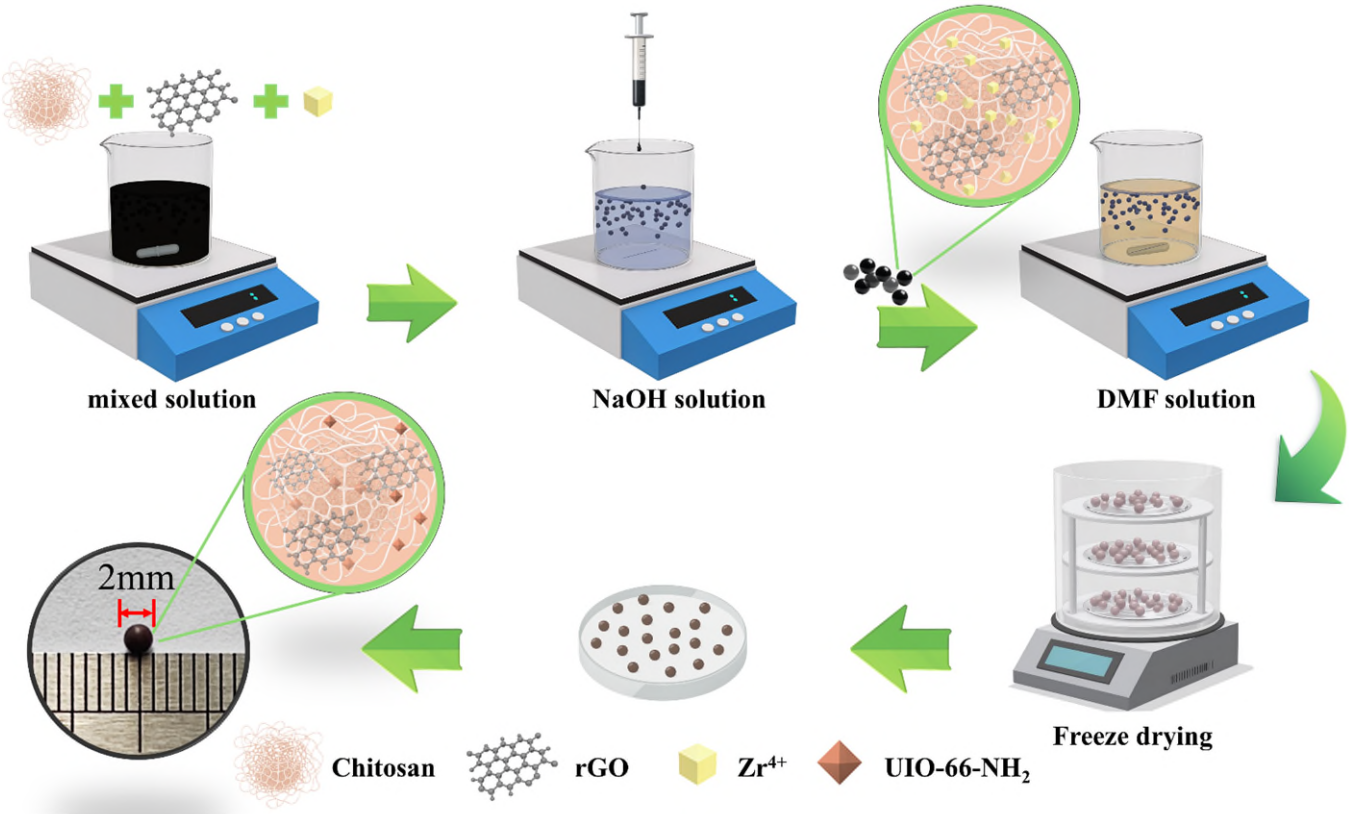
Table 2. Comparison of reported maximum adsorption capacities for TC and NOR across various adsorbent materials.

Antibiotic	Adsorbents	q_m(mg·g^{-1})	Temp. (K)	pH	References
TC	RBC	173.61	313	7	(C. Zhao et al., 2020)
	KBC	830.78	318	2	(Fan et al., 2022)
	CS·Fe_3O_4	211.21	293.15	7	(da Silva Bruckmann et al., 2022)
	Porous graphitic biochar	1122.2	Room temperature	/	(Huang et al., 2023)
	Ca-CSB	93.46	298.15	6	(K. Wang et al., 2023)
	NH_2-MIL-101(Cr)@COFs@SA hydrogel beads	252.6	298	7	(S. Zhang et al., 2024)
NOR	CG/Bx/ZnO	1282.05	298	4	(Sharma et al., 2023)
	CMC/MIL-125(Ti)-NH_2 composite	1251.8	328	3–10	(Peng et al., 2025)
	CA/CTS-M	310.6	NR	NR	(J. Tang et al., 2023)
	3K-SCB750	157.4	313	5	(Yan Zhou et al., 2023)
NOR	Bamboo chopsticks biochar	105.19	318	6	(M. Zhang et al., 2023)

Table 3. Thermodynamic analysis of TC and NOR adsorption behavior

吸附质	温度（K)	ΔG°（kJ/mol)	ΔH°（kJ/mol)	ΔS°（J/mol·K)
TC	293	-22.77	2.52	86.32
	303	-23.64		
	313	-24.49		
NOR	293	-22.78	22.88	155.83
	303	-24.45		
	313	-25.90		

Figure captions



Scheme 1. Preparation strategy and structural assembly process of CS@UiO-66-NH_2@rGO beads.

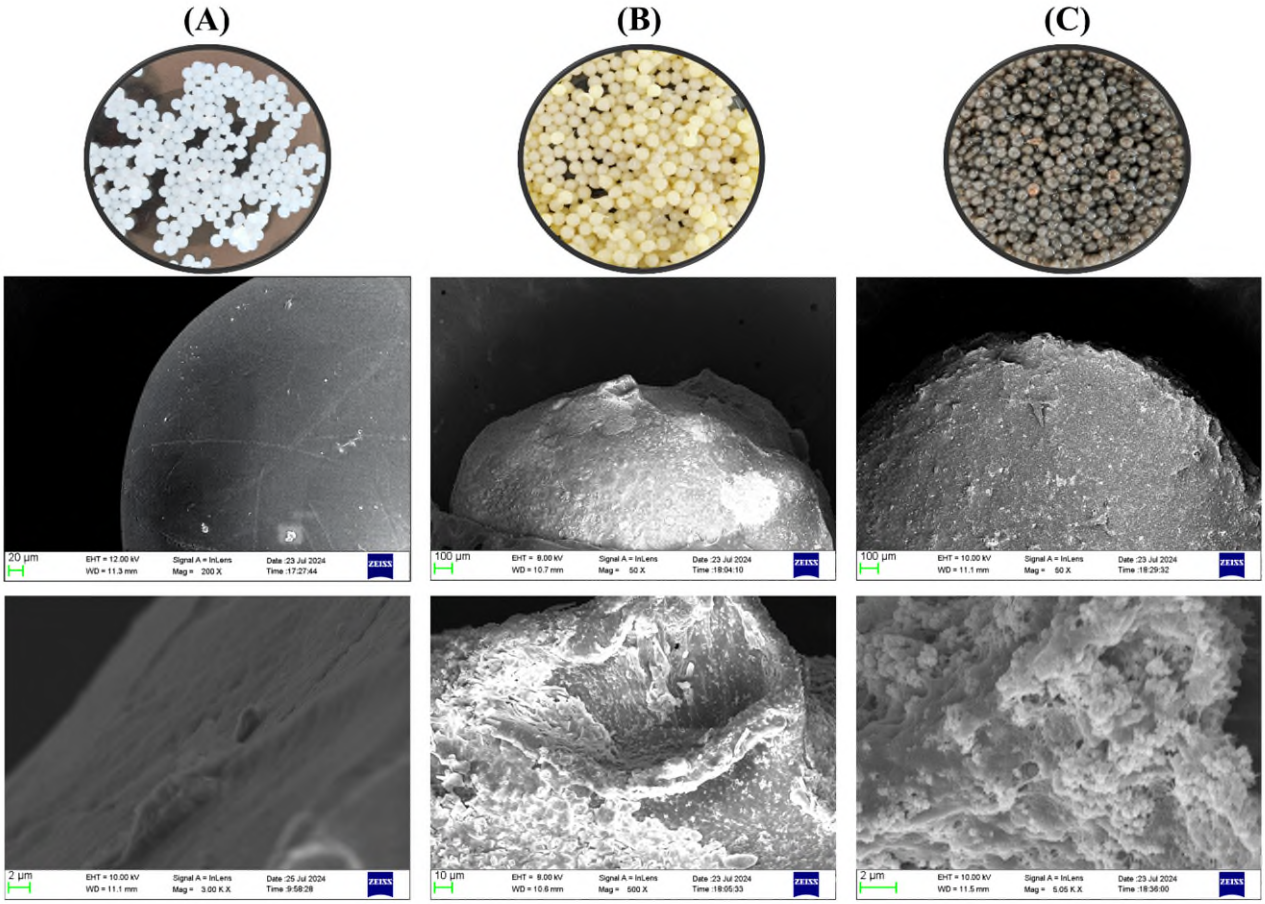


Fig. 1. SEM images of pristine CS beads (A), CS@UiO-66-NH_2 composite beads (B), and CS@UiO-66-NH_2@rGO composite beads (C) under various magnification levels.

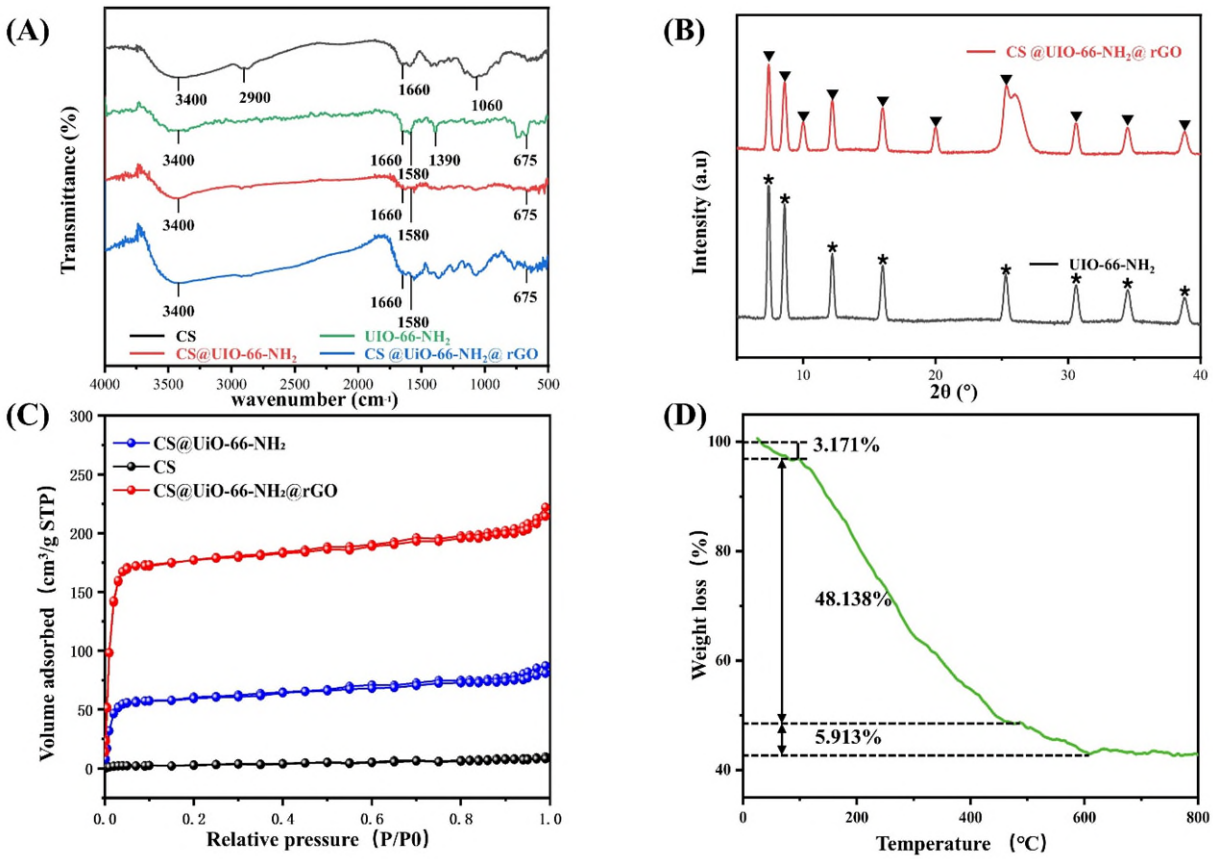


Fig. 2. (A) FTIR spectra of CS, UiO-66-NH_2, CS@UiO-66-NH_2, and CS@UiO-66-NH_2@rGO; (B) XRD patterns of UiO-66-NH_2 and CS@UiO-66-NH_2@rGO; (C) N_2 adsorption–desorption isotherms of CS, CS@UiO-66-NH_2, and CS@UiO-66-NH_2@rGO; (D) TGA curve of CS@UiO-66-NH_2@rGO.

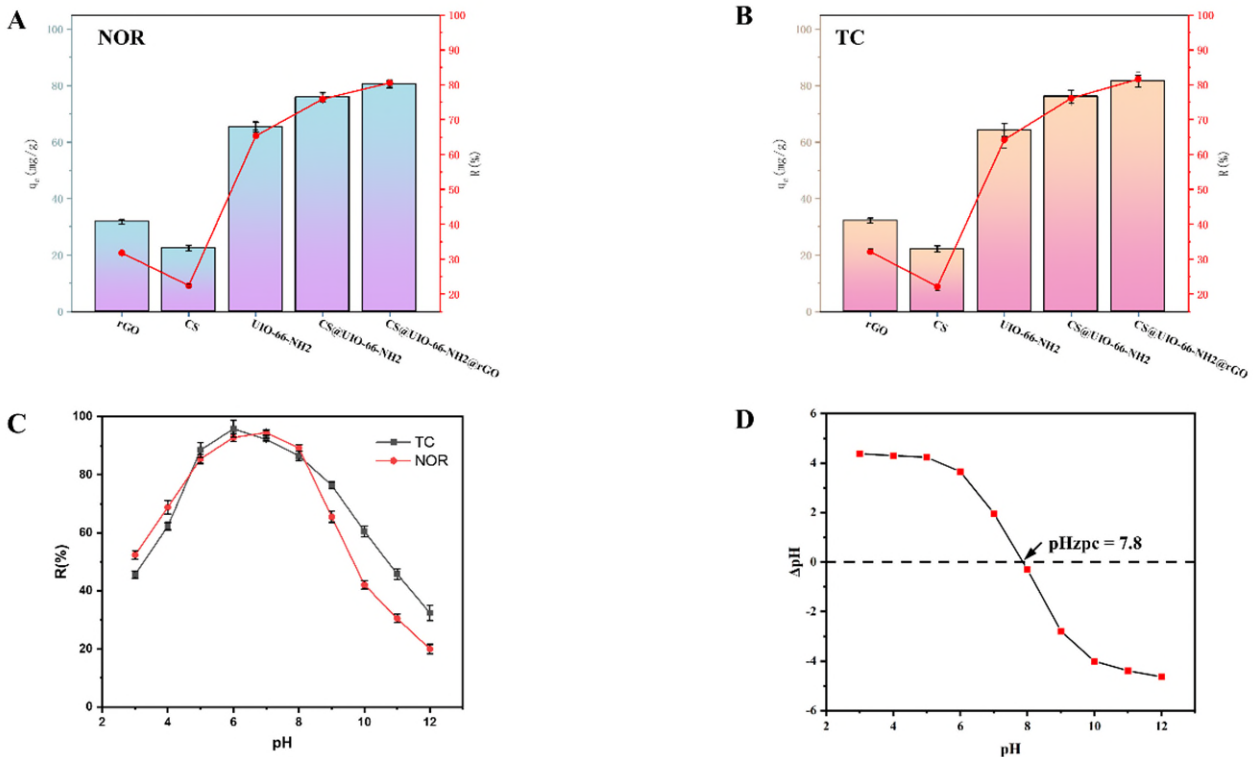


Fig. 3. (A) Adsorption capacity (q_e) and removal efficiency (R) of NOR by different adsorbents (pH = 4, C_0 = 50 mg·L^{-1}, T = 303 K); (B) Adsorption capacity (q_e) and removal efficiency (R) of TC by different adsorbents (pH = 4, C_0 = 50 mg·L^{-1}, T = 303 K); (C) Effect of initial pH (3–12) on the removal efficiency of NOR and TC by CS@UiO-66-NH$_2$@rGO (C_0 = 50 mg·L^{-1}, T = 303 K); (D) ΔpH–pH$_0$ curve for determining the point of zero charge (pH$_p$zc) of CS@UiO-66-NH$_2$@rGO.

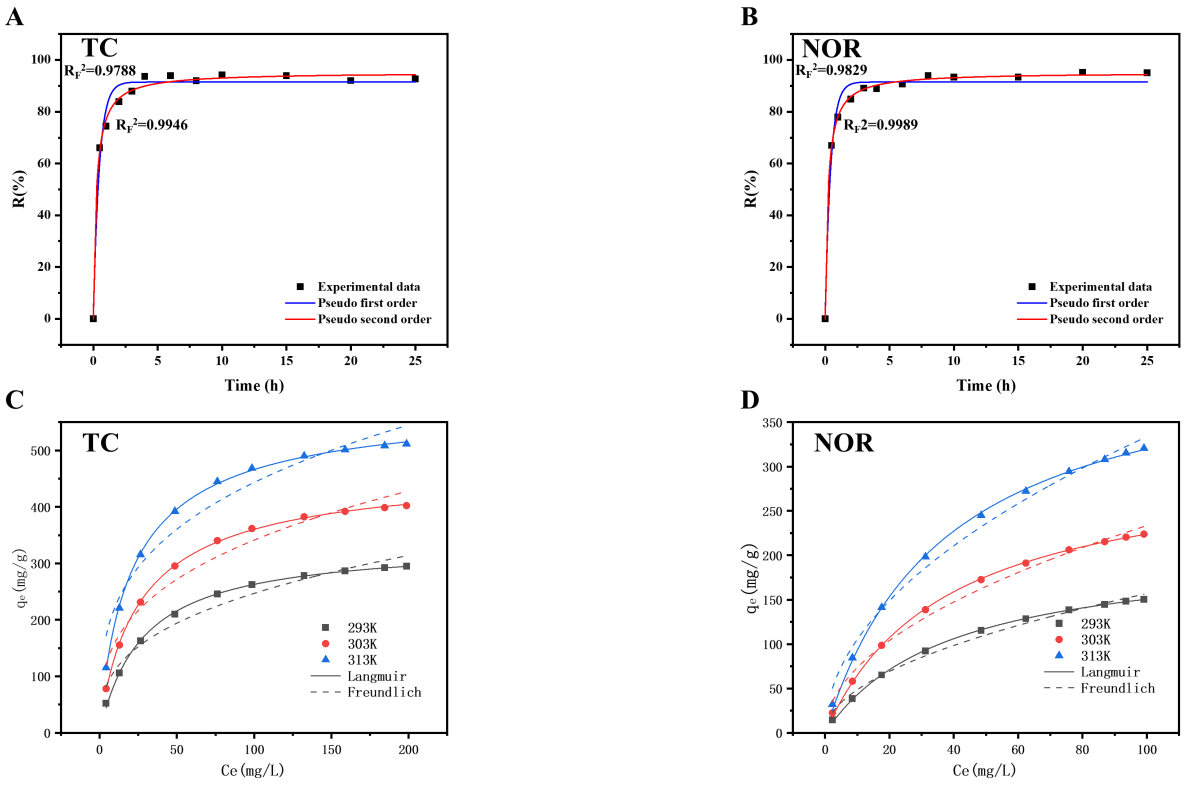


Fig. 4. (A) Adsorption kinetic curves and model fitting (PFO and PSO) for TC on CS@UiO-66-NH_2@rGO (C_0 = 50 mg·L^{-1}, T = 303 K); (B) Adsorption kinetic curves and model fitting for NOR on CS@UiO-66-NH_2@rGO (C_0 = 50 mg·L^{-1}, T = 303 K); (C) Adsorption isotherms and Langmuir/Freundlich fitting for TC at different temperatures (293–313 K); (D) Adsorption isotherms and Langmuir/Freundlich fitting for NOR at different temperatures (293–313 K).

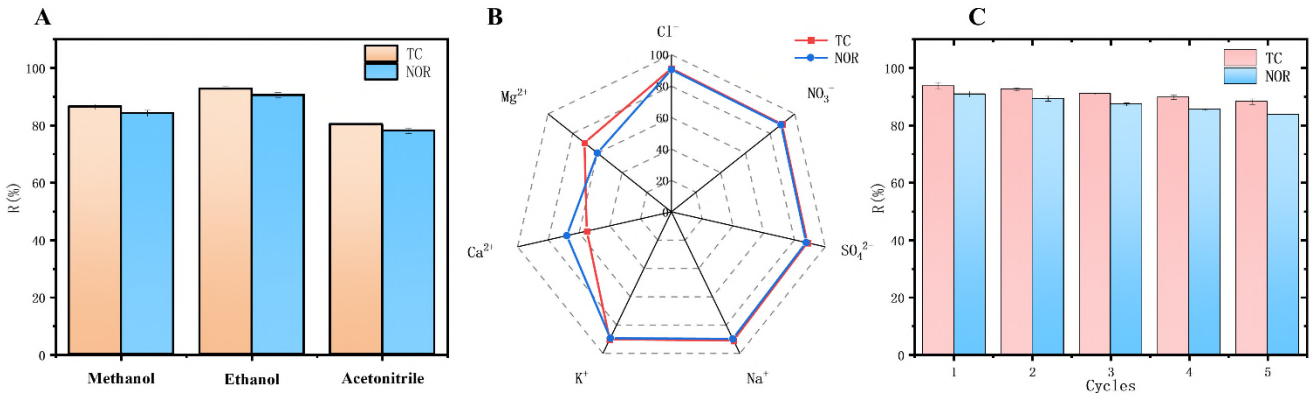


Fig. 5. (A) Effect of different organic solventson the removal efficiency of TC and NOR by CS@UiO-66-NH_2@rGO (C_0 = 50 mg·L^{-1}, T = 303 K); (B) Influence of coexisting inorganic ionson the removal efficiency of TC and NOR; (C) Adsorption–desorption cycles of CS@UiO-66-NH_2@rGO for TC and NOR over five successive runs;

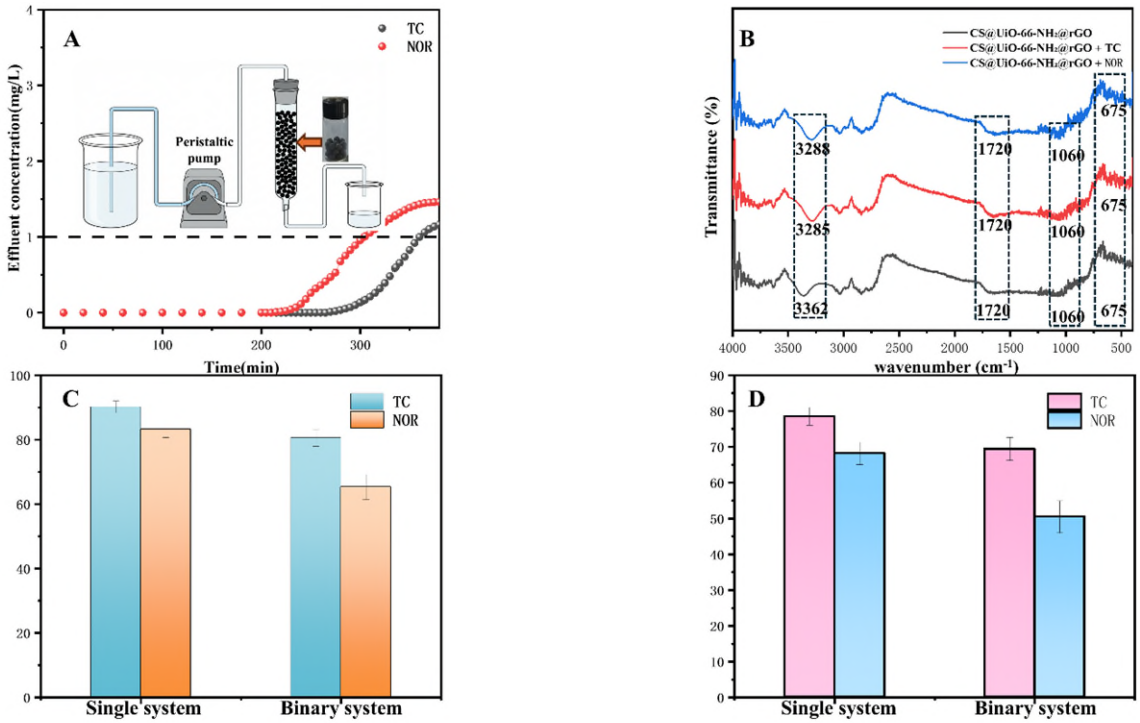


Fig. 6. (A) Breakthrough curves of TC and NOR in fixed-bed columns packed with CS@UiO-66-NH_2@rGO under continuous-flow conditions (C_0 = 20 mg·L^{-1}, flow rate = 1.25 mL·min^{-1}, adsorbent mass = 100 mg, T = 308 K); (B) FTIR spectra of CS@UiO-66-NH_2@rGO before and after adsorption of TC and NOR; (C) Comparison of removal efficiencies of TC and NOR in single and binary systems under batch conditions; (D) Comparison of removal efficiencies of TC and NOR in single and binary systems under dynamic conditions.

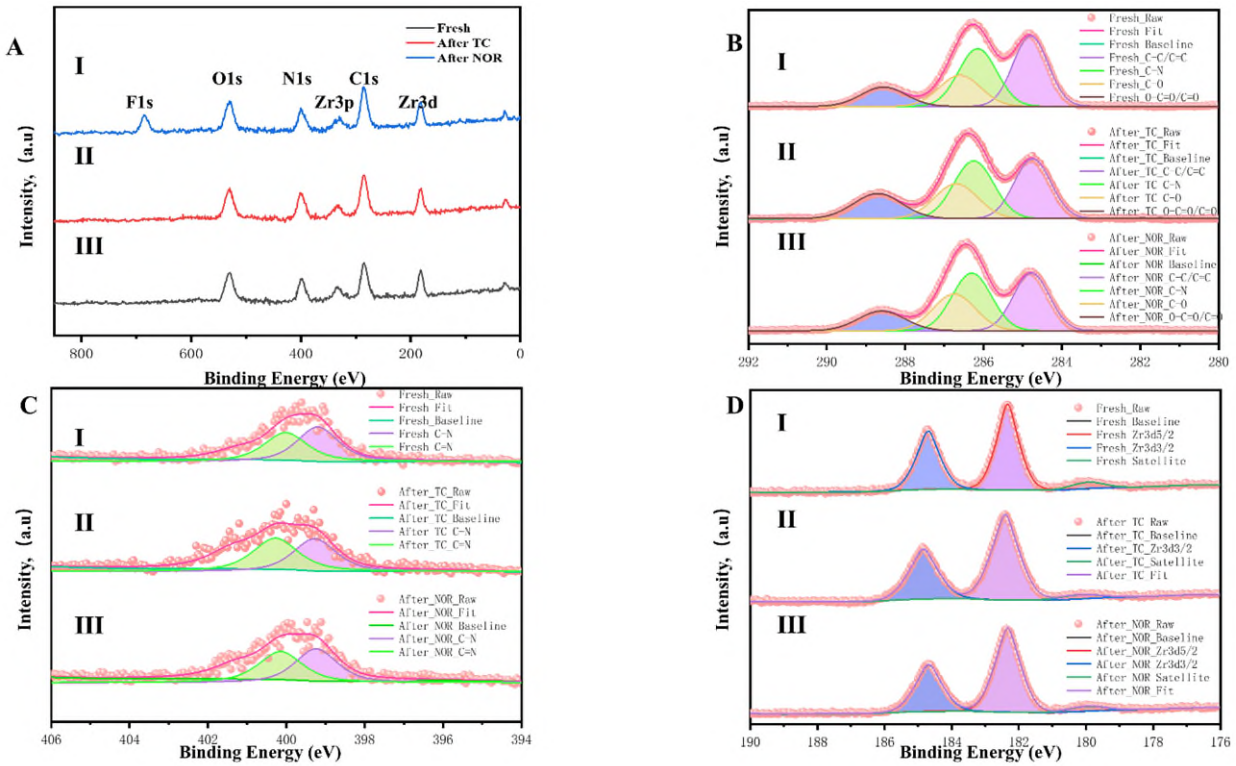


Fig. 7. XPS characterization of CS@UiO-66-NH_2@rGO in its pristine state (I) and following adsorption of TC (II) and NOR (III), including: (A) wide-scan spectrum; (B) detailed C 1s region; (C) detailed N 1s region; and (D) Zr 3d core-level analysis.

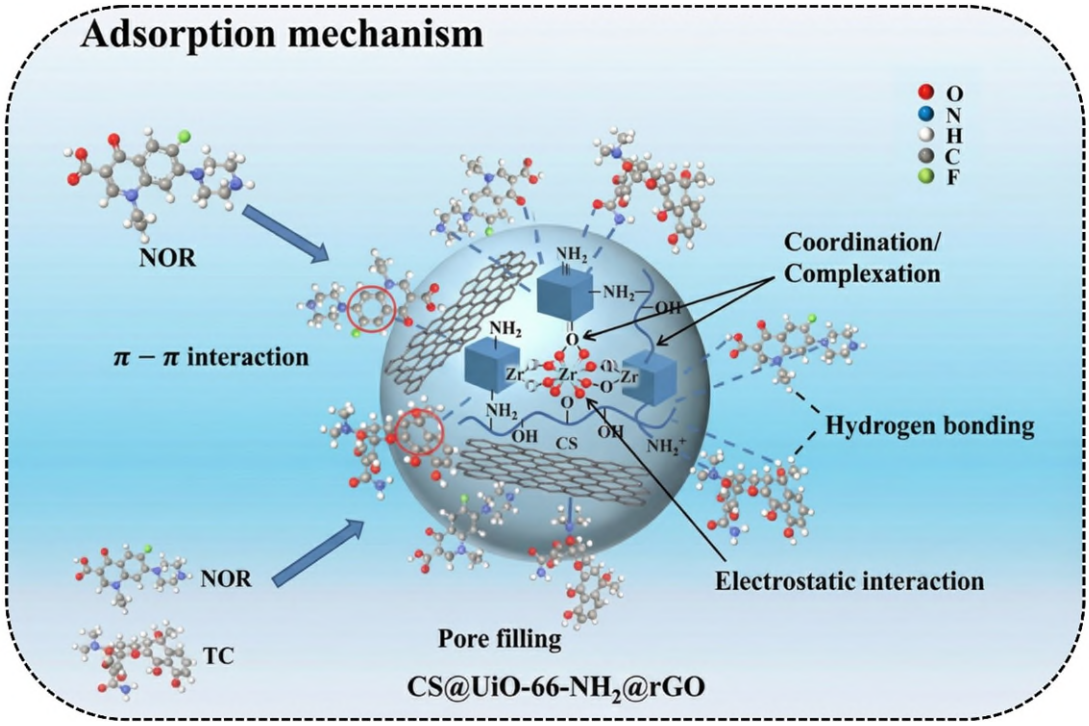


Fig.8. Proposed adsorption mechanism.

References

Abbas, S., Ahmad, K., Naseem, K., Kashif, M., Majeed, H., Qureshi, K., & Ashfaq, M. (2025). Cutting-edge metal-organic frameworks: Revolutionizing the adsorptive removal of pharmaceutical contaminants from water. Reviews in Inorganic Chemistry, 45, 885–905. https://doi.org/10.1515/revic-2024-0119

Abdalkarim, K. A., Tofiq, D. I., Hamarawf, R. F., Hassan, H. Q., Ahmad, B. S., Muhammad, D. S., & Aziz, S. B. (2025). MOF/chitosan composites: An emerging class of multifunctional materials for diverse applications. Journal of Inorganic and Organometallic Polymers and Materials, 35, 4189–4241. https://doi.org/10.1007/s10904-024-03572-9

Abdelfatah, A. M., El-Maghrabi, N., Mahmoud, A. E. D., & Fawzy, M. (2022). Synergetic effect of green synthesized reduced graphene oxide and nano-zero valent iron composite for the removal of doxycycline antibiotic from water. Scientific Reports, 12, 19372. https://doi.org/10.1038/s41598-022-23684-x

Abdi, J., & Abedini, H. (2020). MOF-based polymeric nanocomposite beads as an efficient adsorbent for wastewater treatment in batch and continuous systems: Modelling and experiment. Chemical Engineering Journal, 400, 125862. https://doi.org/10.1016/j.cej.2020.125862

Abdullah, Z., & Ahmed, S. (2025). Recent innovations in nanocomposite beads for the removal of pollutants from water: A critical review. Environmental Science: Water Research & Technology, 11, 1428–1445. https://doi.org/10.1039/D5EW00215J

Abou-Elyazed, A. S., Li, X., & Meng, J. (2024). Engineering ion affinity of Zr-MOF hybrid PDMS membranes for the selective separation of Na+/Ca2+. *Molecules, 29*, 5297. https://doi.org/10.3390/molecules29225297

Abumelha, H. M., Alzahrani, S. O., Alrefaee, S. H., Al-Bonayan, A. M., Alkhatib, F., Saad, F. A., & El-Metwaly, N. M. (2023). Evaluation of tetracycline removal by magnetic metal organic framework from aqueous solutions: Adsorption isotherm, kinetics, thermodynamics, and Box–Behnken design optimization. *Journal of Saudi Chemical Society, 27*, 101706. https://doi.org/10.1016/j.jscs.2023.101706

Adebisi, Y. A. (2023). Balancing the risks and benefits of antibiotic use in a globalized world: The ethics of antimicrobial resistance. *Globalization and Health, 19*, 27. https://doi.org/10.1186/s12992-023-00930-z

Aguila-Rosas, J., Cano, F. J., Nagaya, A., Quirino-Barreda, C. T., de Jesús Martínez Ortiz, M., Vargas, A. G., & Lima, E. (2025). MOF-composites for adsorption and degradation of contaminants in wastewater. *Chemical Communications, 61*, 11706–11731. https://doi.org/10.1039/D5CC02843D

Ahmadijokani, F., Ghaffarkhah, A., Molavi, H., Dutta, S., Lu, Y., Wuttke, S., & Arjmand, M. (2024). COF and MOF hybrids: Advanced materials for wastewater treatment. *Advanced Functional Materials, 34*, 2305527. https://doi.org/10.1002/adfm.202305527

Alamgir, T., Wang, B., Liu, J. H., Ullah, R., Feng, F., & Li, J. R. (2020). Effective adsorption of metronidazole antibiotic from water with a stable Zr(IV)-MOFs:

Insights from DFT, kinetics and thermodynamics studies. *Journal of Environmental Chemical Engineering, 8*, 103642. https://doi.org/10.1016/j.jece.2019.103642

Ali, M. A. M., El-Sayed, M., El-Shamy, O. A. A., Khedr, G. E., Sabaa, M. W., Mohamed, R. R., & Mubarak, M. F. (2025). Eco-friendly composite membranes of recycled PVC and Co-MOFs for efficient Ca2+ scale removal and anti-fouling in water treatment. *Process Safety and Environmental Protection, 202*, 107780. https://doi.org/10.1016/j.psep.2025.107780

Alnajrani, M. N., & Alsager, O. A. (2020). Removal of antibiotics from water by polymer of intrinsic microporosity: Isotherms, kinetics, thermodynamics, and adsorption mechanism. *Scientific Reports, 10*, 794. https://doi.org/10.1038/s41598-020-57616-4

Aziz, K., Raza, N., Kanwal, N., Khairy, M., Ahmadi, Y., & Kim, K. H. (2025). Recent advances in nanomaterial-based adsorbents for removal of pharmaceutical pollutants from wastewater. *Materials Horizons, 12*, 6043–6068. https://doi.org/10.1039/D5MH00627A

Badri, H., Jaafari, J., Khorshidi, A., & Ashrafi, S. D. (2025). Enhanced adsorption of ceftriaxone and cefixime antibiotics via functionalised UiO-66 MOFs (−NH2/−SO3H): Characterisation, isotherm, kinetic-thermodynamic, optimisation and modelling using response surface methodology. *International Journal of Environmental Analytical Chemistry*, 1–23. https://doi.org/10.1080/03067319.2025.2553931

Balakrishnan, A., Appunni, S., Chinthala, M., Jacob, M. M., Vo, D. V. N., Reddy, S. S., & Kunnel, E. S. (2023). Chitosan-based beads as sustainable adsorbents for wastewater remediation: A review. *Environmental Chemistry Letters, 21*, 1881–1905. https://doi.org/10.1007/s10311-023-01563-9

Bathula, S., Thottathil, S., & Puttaiahgowda, Y. M. (2025). MOFs and MOF-based composites for the adsorptive removal of ciprofloxacin. *Macromolecular Materials and Engineering, 310*, 2400238. https://doi.org/10.1002/mame.202400238

Bento, C. S. A., Ruivo, J. P., Alarico, S., Empadinhas, N., Candeias, E., Cardoso, S., & Braga, M. E. M. (2025). Eco-friendly development of sterile chitosan-based aerogels for wound dressing applications using integrated scCO2 processing. *International Journal of Pharmaceutics, 683*, 126021. https://doi.org/10.1016/j.ijpharm.2025.126021

Bhattacharyya, P., Basak, S., & Chakrabarti, S. (2021). Advancement towards antibiotic remediation: Heterostructure and composite materials. *ChemistrySelect, 6*, 7323–7345. https://doi.org/10.1002/slct.202100436

Bi, W., Wang, G., & Hu, X. (2022). Fabrication of Zn-MOF derived graphitic carbon materials with mesoporous structure for adsorptive removal of ceftazidime from aqueous solutions. *Colloids and Surfaces A: Physicochemical and Engineering Aspects, 652*, 129758. https://doi.org/10.1016/j.colsurfa.2022.129758

Bouaziz, N., Kouira, O., Aouaini, F., Bukhari, L., Knani, S., Znaidia, S., & Lamine, A. B. (2023). Adsorption of antibiotics by bentonite-chitosan composite: Phenomenological modeling and physical investigation of the adsorption process.

International Journal of Biological Macromolecules, 242, 125156. https://doi.org/10.1016/j.ijbiomac.2023.125156

Cai, G., Yan, P., Zhang, L., Zhou, H. C., & Jiang, H. L. (2021). Metal–organic framework-based hierarchically porous materials: Synthesis and applications. *Chemical Reviews, 121*, 12278–12326. https://doi.org/10.1021/acs.chemrev.1c00243

Calderon Moreno, J. M., Chelu, M., & Popa, M. (2025). Biocompatible stimuli-sensitive natural hydrogels: Recent advances in biomedical applications. *Gels, 11*, 993. https://doi.org/10.3390/gels11120993

Carrales-Alvarado, D. H., Rodríguez-Ramos, I., Leyva-Ramos, R., Mendoza-Mendoza, E., & Villela-Martínez, D. E. (2020). Effect of surface area and physical–chemical properties of graphite and graphene-based materials on their adsorption capacity towards metronidazole and trimethoprim antibiotics in aqueous solution. *Chemical Engineering Journal, 402*, 126155. https://doi.org/10.1016/j.cej.2020.126155

Chai, Y., Zhang, Y., Wang, L., Du, Y., Wang, B., Li, N., & Ou, L. (2022). In situ one-pot construction of MOF/hydrogel composite beads with enhanced wastewater treatment performance. *Separation and Purification Technology, 295*, 121225. https://doi.org/10.1016/j.seppur.2022.121225

Chen, B., Li, Y., Li, M., Cui, M., Xu, W., Li, L., & Chen, K. (2021). Rapid adsorption of tetracycline in aqueous solution by using MOF-525/graphene oxide composite. *Microporous and Mesoporous Materials, 328*, 111457. https://doi.org/10.1016/j.micromeso.2021.111457

Cheng, P., Wang, C., Kaneti, Y. V., Eguchi, M., Lin, J., Yamauchi, Y., & Na, J. (2020). Practical MOF nanoarchitectonics: New strategies for enhancing the processability of MOFs for practical applications. *Langmuir, 36*, 4231–4249. https://doi.org/10.1021/acs.langmuir.0c00236

da Silva Bruckmann, F., Schnorr, C. E., da Rosa Salles, T., Nunes, F. B., Baumann, L., Müller, E. I., & Bohn Rhoden, C. R. (2022). Highly efficient adsorption of tetracycline using chitosan-based magnetic adsorbent. *Polymers, 14*, 4854. https://doi.org/10.3390/polym14224854

de Ilurdoz, M. S., Sadhwani, J. J., & Reboso, J. V. (2022). Antibiotic removal processes from water and wastewater for the protection of the aquatic environment: A review. *Journal of Water Process Engineering, 45*, 102474. https://doi.org/10.1016/j.jwpe.2021.102474

Deng, H., Wu, Y., Li, L., Jiang, X., Wang, P., Fang, K., & Li, Q. (2025). Synergistic mechanisms for efficient and safe antibiotic removal: Effective adsorption and photocatalytic degradation using aerogels. *Separation and Purification Technology, 354*, 129455. https://doi.org/10.1016/j.seppur.2024.129455

Djidja, R., Dewez, D., & Azzouz, A. (2025). Norfloxacin oxidative degradation and toxicity in aqueous media: Reciprocal effects of acidity evolution on metal cations and clay catalyst dispersion. *International Journal of Molecular Sciences, 26*, 4347. https://doi.org/10.3390/ijms26094347

Dutta, J., & Mala, A. A. (2020). Removal of antibiotic from the water environment by the adsorption technologies: A review. *Water Science and Technology, 82*, 401–426. https://doi.org/10.2166/wst.2020.335

Ezzati, R. (2024). A new insight into the pseudo-first-order model: Investigation of the adsorption mechanism of amoxicillin, diclofenac sodium, and methylene blue on various adsorbents based on the pseudo-first-order rate constant. *Chemical Engineering Communications, 211*, 1129–1138. https://doi.org/10.1080/00986445.2024.2336232

Fakhraei Ghazvini, M., Vahedi, M., Najafi Nobar, S., & Sabouri, F. (2021). Investigation of the MOF adsorbents and the gas adsorptive separation mechanisms. *Journal of Environmental Chemical Engineering, 9*, 104790. https://doi.org/10.1016/j.jece.2020.104790

Fan, Z., Fang, J., Zhang, G., Qin, L., Fang, Z., & Jin, L. (2022). Improved adsorption of tetracycline in water by a modified *Caulis spatholobi* residue biochar. *ACS Omega, 7*, 30543–30553. https://doi.org/10.1021/acsomega.2c04033

Fang, X., Wu, S., Wu, Y., Yang, W., Li, Y., He, J., & Liu, J. (2020). High-efficiency adsorption of norfloxacin using octahedral UiO-66-NH2 nanomaterials: Dynamics, thermodynamics, and mechanisms. *Applied Surface Science, 518*, 146226. https://doi.org/10.1016/j.apsusc.2020.146226

Farahbakhsh, J., Golgoli, M., Najafi, M., Haeri, S. Z., Khiadani, M., Razmjou, A., & Zargar, M. (2025). An innovative NH2-UiO-66/NH2-MIL-125 MOF-on-MOF structure to improve the performance and antifouling properties of ultrafiltration

membranes. *Separation and Purification Technology, 353*, 128273. https://doi.org/10.1016/j.seppur.2024.128273

Frey, L., Tanunchai, B., & Glaser, B. (2022). Antibiotics residues in pig slurry and manure and its environmental contamination potential: A meta-analysis. *Agronomy for Sustainable Development, 42*, 31. https://doi.org/10.1007/s13593-022-00762-y

Gaballah, M. S., Sobhi, M., Guo, J., Philbert, M., Min, L., Zheng, Y., & Dong, R. (2023). Evaluating the removal and impacts of combined tetracycline, oxytetracycline, sulfadiazine, and norfloxacin during swine manure storage process at ambient temperatures. *Journal of Environmental Chemical Engineering, 11*, 109765. https://doi.org/10.1016/j.jece.2023.109765

Gai, S., Zhang, J., Fan, R., Xing, K., Chen, W., Zhu, K., & Yang, Y. (2020). Highly stable zinc-based metal–organic frameworks and corresponding flexible composites for removal and detection of antibiotics in water. *ACS Applied Materials & Interfaces, 12*, 8650–8662. https://doi.org/10.1021/acsami.9b19583

Gan, W., Zheng, Z., Yan, J., He, X., Zhuang, Z., Chen, F. F., & Yu, Y. (2024). Vertical MOF film supported on an organic–inorganic mixed substrate for complex wastewater purification. *Applied Surface Science, 652*, 159253. https://doi.org/10.1016/j.apsusc.2023.159253

Gao, Y., Zheng, L., Duan, L., & Bi, J. (2024). Separable metal–organic framework-based materials for the adsorption of emerging contaminants. *Langmuir, 40*, 15365–15388. https://doi.org/10.1021/acs.langmuir.4c01308

Gaspari, S., Akkermans, S., Akritidou, T., Whelan, R., Devine, F., & Van Impe, J. F. M. (2024). Interference of gastrointestinal barriers with antibiotic susceptibility of foodborne pathogens: An in vitro case study of ciprofloxacin and tetracycline against *Salmonella enterica* and *Listeria monocytogenes*. *Food Research International, 188*, 114491. https://doi.org/10.1016/j.foodres.2024.114491

Ge, L., Zhang, M., Wang, R., Li, N., Zhang, L., Liu, S., & Jiao, T. (2020). Fabrication of CS/GA/RGO/Pd composite hydrogels for highly efficient catalytic reduction of organic pollutants. *RSC Advances, 10*, 15091–15097. https://doi.org/10.1039/D0RA01884H

Ghaedi, S., Rajabi, H., Hadi Mosleh, M., & Sedighi, M. (2025). MOF biochar composites for environmental protection and pollution control. *Bioresource Technology, 418*, 131982. https://doi.org/10.1016/j.biortech.2024.131982

Guo, F., Wang, D., Wu, H., Zhao, X., Xu, F., Cui, Y., & Wen, T. (2025). Genomic characteristics, antimicrobial resistance profiles and virulence factors of *Gallibacterium anatis* isolates from layer chickens in Northern China. *BMC Microbiology, 25*, 706. https://doi.org/10.1186/s12866-025-04440-3

Guo, X., Pan, Y., Xie, Y., & Cai, P. (2026). Sodium alginate/carboxymethyl chitosan composite hydrogel beads for pH/redox dual-responsive pesticide release. *Reactive and Functional Polymers, 221*, 106659. https://doi.org/10.1016/j.reactfunctpolym.2026.106659

Guo, Y., Huang, J., Yang, W., & Xu, H. (2025). PAA-functionalized UiO-66 incorporated into lotus biochar-chitosan hydrogel: A bimetallic adsorbent with

enhanced adsorption capacity for antibiotics. *Colloids and Surfaces A: Physicochemical and Engineering Aspects, 727*, 138127. https://doi.org/10.1016/j.colsurfa.2025.138127

Ha, H. Q., Nguyen, N. P. T., Nguyen, T. T. T., & Tran, T. V. (2025). Removal of selected antibiotics and anti-inflammatory drugs using metal–organic framework-based adsorbents. *Journal of Industrial and Engineering Chemistry*. https://doi.org/10.1016/j.jiec.2025.08.049

Haenni, M., Dagot, C., Chesneau, O., Bibbal, D., Labanowski, J., Vialette, M., & Hocquet, D. (2022). Environmental contamination in a high-income country (France) by antibiotics, antibiotic-resistant bacteria, and antibiotic resistance genes: Status and possible causes. *Environment International, 159*, 107047. https://doi.org/10.1016/j.envint.2021.107047

Hao, D., Song, Y. X., Zhang, Y., & Fan, H. T. (2021). Nanocomposites of reduced graphene oxide with pure monoclinic-ZrO2 and pure tetragonal-ZrO2 for selective adsorptive removal of oxytetracycline. *Applied Surface Science, 543*, 148810. https://doi.org/10.1016/j.apsusc.2020.148810

He, T., Kong, X. J., & Li, J. R. (2021). Chemically stable metal–organic frameworks: Rational construction and application expansion. *Accounts of Chemical Research, 54*, 3083–3094. https://doi.org/10.1021/acs.accounts.1c00280

Hooriabad Saboor, F., Nasirpour, N., Shahsavari, S., & Kazemian, H. (2022). The effectiveness of MOFs for the removal of pharmaceuticals from aquatic

environments: A review focused on antibiotics removal. *Chemistry – An Asian Journal, 17*, e202101105. https://doi.org/10.1002/asia.202101105

Hosono, N., & Uemura, T. (2021). Metal–organic frameworks as versatile media for polymer adsorption and separation. *Accounts of Chemical Research, 54*, 3593–3603. https://doi.org/10.1021/acs.accounts.1c00377

Hou, J., Sapnik, A. F., & Bennett, T. D. (2020). Metal–organic framework gels and monoliths. *Chemical Science, 11*, 310–323. https://doi.org/10.1039/C9SC04961D

Hu, S. Z., Huang, T., Zhang, N., Lei, Y. Z., & Wang, Y. (2022). Chitosan-assisted MOFs dispersion via covalent bonding interaction toward highly efficient removal of heavy metal ions from wastewater. *Carbohydrate Polymers, 277*, 118809. https://doi.org/10.1016/j.carbpol.2021.118809

Huang, B., Huang, D., Zheng, Q., Yan, C., Feng, J., Gao, H., & Liao, Y. (2023). Enhanced adsorption capacity of tetracycline on porous graphitic biochar with an ultra-large surface area. *RSC Advances, 13*, 10397–10407. https://doi.org/10.1039/D3RA00745F

Imanipoor, J., Mohammadi, M., Dinari, M., & Ehsani, M. R. (2021). Adsorption and desorption of amoxicillin antibiotic from water matrices using an effective and recyclable MIL-53(Al) metal–organic framework adsorbent. *Journal of Chemical & Engineering Data, 66*, 389–403. https://doi.org/10.1021/acs.jced.0c00736

Isaeva, V. I., Vedenyapina, M. D., Kurmysheva, A. Y., Weichgrebe, D., Nair, R. R., Nguyen, N. P., & Kustov, L. M. (2021). Modern carbon-based materials for

adsorptive removal of organic and inorganic pollutants from water and wastewater. *Molecules, 26*, 6628. https://doi.org/10.3390/molecules26216628

Istirokhatun, T., Fajrina, A. N., Susanto, H., Gonzales, R. R., Desiriani, R., & Matsuyama, H. (2025). UiO-66-NH2: Sourcing amino groups from natural material and their application in membranes for water contaminants removal. *Chemical Engineering Journal, 509*, 160183. https://doi.org/10.1016/j.cej.2025.160183

Jansen, C., Tran-Cong, N. M., Schlüsener, C., Schmitz, A., Proksch, P., & Janiak, C. (2022). MOF@chitosan composites with potential antifouling properties for open-environment applications of metal-organic frameworks. *Solids, 3*, 35–54. https://doi.org/10.3390/solids3010004

Jin, R., Gong, J., Li, Z., Xiang, B., Liu, W., & Li, J. (2026). “Corn-like” APT@UiO-66-NH2/PEG composite membrane with excellent anti-fouling performance for oil/water emulsions separation. *Separation and Purification Technology, 386*, 136557. https://doi.org/10.1016/j.seppur.2025.136557

Kang, F., Pan, J., Deng, J., Zhang, T., Ren, S., Zhang, L., & Tu, J. (2025). Synergistic effect of UiO-66-NH2 and modified steel slag on flame retardancy and smoke suppression of silicone rubber foam. *Applied Materials Today, 47*, 102927. https://doi.org/10.1016/j.apmt.2025.102927

Kaur, H., Devi, N., Siwal, S. S., Alsanie, W. F., Thakur, M. K., & Thakur, V. K. (2023). Metal–organic framework-based materials for wastewater treatment: Superior adsorbent materials for the removal of hazardous pollutants. *ACS Omega, 8*, 9004–9030. https://doi.org/10.1021/acsomega.2c07719

Keshvardoostchokami, M., Majidi, M., Zamani, A., & Liu, B. (2021). A review on the use of chitosan and chitosan derivatives as the bio-adsorbents for the water treatment: Removal of nitrogen-containing pollutants. *Carbohydrate Polymers, 273*, 118625. https://doi.org/10.1016/j.carbpol.2021.118625

Khan, N. A., Shaheen, S., Najam, T., Shah, S. S. A., Javed, M. S., Nazir, M. A., & Ashfaq, M. (2021). Efficient removal of norfloxacin by MOF@GO composite: Isothermal, kinetic, statistical, and mechanistic study. *Toxin Reviews, 40*, 915–927. https://doi.org/10.1080/15569543.2020.1801750

Khezerlou, A., Tavassoli, M., Abedi-Firoozjah, R., Alizadeh Sani, M., Ehsani, A., & Varma, R. S. (2025). MOFs-based adsorbents for the removal of tetracycline from water and food samples. *Scientific Reports, 15*, 502. https://doi.org/10.1038/s41598-024-84122-8

Kweon, J., Lee, H., Kim, S., & Song, G. (2025). Environmental antibiotic emissions and their residual impact on livestock farming. *Molecular & Cellular Toxicology, 21*, 351–362. https://doi.org/10.1007/s13273-024-00504-z

Larsson, D. G. J., & Flach, C. F. (2022). Antibiotic resistance in the environment. *Nature Reviews Microbiology, 20*, 257–269. https://doi.org/10.1038/s41579-021-00649-x

Li, J., Lin, G., Zhong, Z., Wang, Z., Wang, S., Fu, L., & Hu, T. (2024). A novel magnetic Ti-MOF/chitosan composite for efficient adsorption of Pb(II) from aqueous solutions: Synthesis and investigation. *International Journal of Biological Macromolecules, 258*, 129170. https://doi.org/10.1016/j.ijbiomac.2023.129170

Li, N., Pang, J., Lang, F., & Bu, X. H. (2024). Flexible metal–organic frameworks: From local structural design to functional realization. *Accounts of Chemical Research, 57*, 2279–2292. https://doi.org/10.1021/acs.accounts.4c00253

Li, R., Huang, D., Lei, L., Chen, S., Chen, Y., Wang, G., & Chen, H. (2023). Lignin and metal–organic frameworks: Mutual partners on the road to sustainability. *Journal of Materials Chemistry A, 11*, 2595–2617. https://doi.org/10.1039/D2TA09241G

Li, Z., Liu, C., Frick, J. J., Davey, A. K., Dods, M. N., Carraro, C., & Maboudian, R. (2023). Synthesis and characterization of UiO-66-NH2 incorporated graphene aerogel composites and their utilization for absorption of organic liquids. *Carbon, 201*, 561–567. https://doi.org/10.1016/j.carbon.2022.09.015

Li, Z., Mao, X., Yu, Y., Zhu, N., Liu, H., Xu, N., & Zhao, J. (2022). Novel metal–organic framework materials in-focus detection and adsorption cues for environmental pollutants. *Reviews of Environmental Contamination and Toxicology, 260*, 16. https://doi.org/10.1007/s44169-022-00020-y

Li, Z., Wang, X., Zhang, X., Yang, Y., & Duan, J. (2021). A high-efficiency and plane-enhanced chitosan film for cefotaxime adsorption compared with chitosan particles in water. *Chemical Engineering Journal, 413*, 127494. https://doi.org/10.1016/j.cej.2020.127494

Liang, Y., Yang, X., Wang, X., Guan, Z. J., Xing, H., & Fang, Y. (2023). A cage-on-MOF strategy to coordinatively functionalize mesoporous MOFs for manipulating selectivity in adsorption and catalysis. *Nature Communications, 14*, 5223. https://doi.org/10.1038/s41467-023-40973-9

Lin, S., Zhao, Z., Lv, J., Guan, L., Du, H., Liang, S. X., & Janiak, C. (2023). Designing a novel metal–organic framework@covalent organic framework composite for the selective removal of fluoroquinolones: Adsorption behaviors and theoretical investigation. *Applied Surface Science, 609*, 155433. https://doi.org/10.1016/j.apsusc.2022.155433

Liu, C., Lin, L., Sun, Q., Wang, J., Huang, R., Chen, W., & Yu, C. (2020). Site-specific growth of MOF-on-MOF heterostructures with controllable nano-architectures: Beyond the combination of MOF analogues. *Chemical Science, 11*, 3680–3686. https://doi.org/10.1039/D0SC00417K

Liu, D., Gu, W., Zhou, L., Lei, J., Wang, L., Zhang, J., & Liu, Y. (2023). From biochar to functions: Lignin induced formation of Fe3C in carbon/Fe composites for efficient adsorption of tetracycline from wastewater. *Separation and Purification Technology, 304*, 122217. https://doi.org/10.1016/j.seppur.2022.122217

Liu, Q., Peng, B., Li, J., Zhao, F., Liu, E., Han, H., & Xing, J. (2025). Double-network carboxymethyl chitosan/chondroitin sulfate hydrogel microspheres prepared by green-LED-triggered droplet photopolymerization for malachite green adsorption. *International Journal of Biological Macromolecules, 322*, 146898. https://doi.org/10.1016/j.ijbiomac.2025.146898

Liu, X., Hong, D., Zhang, D., & Jiang, Y. (2024). Carbon dots-functionalized metal–organic framework for the dual detection of tetracycline and norfloxacin. *Journal of Molecular Structure, 1312*, 138567. https://doi.org/10.1016/j.molstruc.2024.138567

Liu, Z., Chen, G., & Lu, X. (2021). In-situ growth of molecularly imprinted metal–organic frameworks on 3D carbon foam as an efficient adsorbent for selective removal of antibiotics. *Journal of Molecular Liquids, 340*, 117232. https://doi.org/10.1016/j.molliq.2021.117232

Lu, L., & Na, C. (2022). Gibbsian interpretation of Langmuir, Freundlich and Temkin isotherms for adsorption in solution. *Philosophical Magazine Letters, 102*, 239–253. https://doi.org/10.1080/09500839.2022.2084571

Lu, L., Yang, Q., Xu, Q., Sun, Y., Tang, S., Tang, X., & Yu, Y. (2022). Two-dimensional materials beyond graphene for the detection and removal of antibiotics: A critical review. *Critical Reviews in Environmental Science and Technology, 52*, 3493–3524. https://doi.org/10.1080/10643389.2021.1929001

Luo, Q., Liu, P., Bi, L., Shi, L., Zhou, J., Fang, F., & Li, J. (2024). Selective and efficient removal of ciprofloxacin from water by bimetallic MOF beads: Mechanism quantitative analysis and dynamic adsorption. *Separation and Purification Technology, 332*, 125832. https://doi.org/10.1016/j.seppur.2023.125832

Ma, R., Hou, Y., Zhang, W., Pan, Y. T., Huo, S., & Shi, C. (2025). MOF-based nanocomposites in polymer matrix: Progress and prospects. *Advanced Composites and Hybrid Materials, 8*, 351. https://doi.org/10.1007/s42114-025-01435-6

Mi, Z., Liu, X., Zhang, Y., Wang, B., Guo, H., Chen, Y., & Jiang, J. (2025). Constructing carboxylated cellulose nanofibers/chitosan aerogel loading with CdS/UiO-66-NH2 for wastewater treatment: Synergistic adsorption and visible light photocatalytic

degradation. *International Journal of Biological Macromolecules, 315*, 144602. https://doi.org/10.1016/j.ijbiomac.2025.144602

Miao, Q., Jiang, L., Yang, J., Hu, T., Shan, S., Su, H., & Wu, F. (2022). MOF/hydrogel composite-based adsorbents for water treatment: A review. *Journal of Water Process Engineering, 50*, 103348. https://doi.org/10.1016/j.jwpe.2022.103348

Moaty, S. A. A., Kotp, A. A., Salah, A. M., Farghali, A. A., & Eldin, Z. E. (2025). Application of UiO-66 MOF for rifampicin removal and post-adsorption antimicrobial activity against MRSA. *Scientific Reports, 15*, 25768. https://doi.org/10.1038/s41598-025-10145-4

Mojtahedi, F., Nasiri, M. R., Ali, S. N., Mohammadgholi, A., Mohebbi, S., Shahbazi, Z., & Baghbani-Arani, F. (2025). Novel chitosan-alginate dressings with UiO-66-NH2 nanoparticles and *Ferula gummosa* extracts for effective wound healing. *Colloids and Surfaces A: Physicochemical and Engineering Aspects, 719*, 137004. https://doi.org/10.1016/j.colsurfa.2025.137004

More, M. S., Bodkhe, G. A., Ingle, N. N., Singh, F., Tsai, M. L., Kim, M., & Shirsat, M. D. (2023). Metal–organic framework (MOF)/reduced graphene oxide (rGO) composite for high performance CO sensor. *Solid-State Electronics, 204*, 108638. https://doi.org/10.1016/j.sse.2023.108638

Mukherjee, D., Behera, J., Mondal, S., Pal, S. C., Volkmer, D., & Das, M. C. (2023). Critical perspectives on metal–organic frameworks and their composites for the adsorptive removal of antibiotics from wastewater matrices. *Crystal Growth & Design, 23*, 7612–7634. https://doi.org/10.1021/acs.cgd.3c00892

Musarurwa, H., & Tavengwa, N. T. (2022a). Advances in the application of chitosan-based metal organic frameworks as adsorbents for environmental remediation. *Carbohydrate Polymers, 283*, 119153. https://doi.org/10.1016/j.carbpol.2022.119153

Musarurwa, H., & Tavengwa, N. T. (2022b). Smart metal-organic framework (MOF) composites and their applications in environmental remediation. *Materials Today Communications, 33*, 104823. https://doi.org/10.1016/j.mtcomm.2022.104823

Nguyen, T. T., Nguyen, M. K., Kumar, V., Huu Do, H., Thi Kim Le, A., Van Nguyen, A., & Trung, L. G. (2024). Optimal adsorption of pefloxacin antibiotics from aqueous solutions: Improved performance with metal–organic framework MIL-101(Cr). *Colloids and Surfaces A: Physicochemical and Engineering Aspects, 689*, 133642. https://doi.org/10.1016/j.colsurfa.2024.133642

Noori Keshtkar, M., Mousavi, S. A., & Molavi, H. (2025). Effective removal of tetracycline from water using stable MOF-808: A comprehensive investigation on activation, stability, and influencing parameters. *Langmuir, 41*, 13395–13406. https://doi.org/10.1021/acs.langmuir.5c01159

Obeso, J. L., Flores, C. V., Boujnah, M., Viltres, H., Celaya, C. A., Rosas, P. M., & Leyva, C. (2024). Al(III)-based MOF for tetracycline removal from water: Adsorption performance and mechanism. *Journal of Solid State Chemistry, 338*, 124908. https://doi.org/10.1016/j.jssc.2024.124908

Peng, T., Chen, F., Yang, J., Xia, M., Wang, F., Zhu, S., & Wang, F. (2025). High-capacity norfloxacin capture by CMC/MIL-125(Ti)-NH2: One-pot synthesis,

performance, and synergistic mechanisms. *ACS Applied Materials & Interfaces, 17*, 69342–69355. https://doi.org/10.1021/acsami.5c17816

Quan, X., & Zhang, J. (2024). Phosphate adsorption from reclaimed water via external cage expansion on CD-MOF micro-interface. *ACS ES&T Water, 4*, 4793–4805. https://doi.org/10.1021/acsestwater.4c00438

Ram, B., & Kumar, M. (2020). Correlation appraisal of antibiotic resistance with fecal, metal and microplastic contamination in a tropical Indian river, lakes and sewage. *npj Clean Water, 3*, 3. https://doi.org/10.1038/s41545-020-0050-1

Rr, R., & Haimbodi, R. (2026). Recent advances in ZnO/MOFs: Synthesis, characterization, and applications in sustainable antibiotic wastewater treatment. *Chinese Journal of Analytical Chemistry, 54*, 100619. https://doi.org/10.1016/j.cjac.2025.100619

Sallam, S., Alorabi, A. Q., Almotairy, A. R. Z., Ibarhiam, S. F., Aljuhani, E., Al-Qahtani, S. D., & El-Metwaly, N. M. (2023). Superior and effective adsorption of amoxicillin by using novel metal organic framework and its composite: Thermodynamic, kinetic, and optimization by Box–Behnken design. *Applied Organometallic Chemistry, 37*, e7184. https://doi.org/10.1002/aoc.7184

Samrot, A. V., Wilson, S., Sanjay Preeth, R. S., Prakash, P., Sathiyasree, M., Saigeetha, S., & Rajesh, V. V. (2023). Sources of antibiotic contamination in wastewater and approaches to their removal—An overview. *Sustainability, 15*, 12639. https://doi.org/10.3390/su151612639

Sathiyaseelan, A., Zhang, X., Lu, Y., Azeez, N. A., Zhang, L., Krishnakumar, G. S., & Wang, M. H. (2025). Exploring the synthesis, properties, and potential of chitosan-functionalized metal–organic frameworks in emerging applications. *Progress in Materials Science, 148*, 101387. https://doi.org/10.1016/j.pmatsci.2024.101387

Selvam, A., Parmar, P. R., Bandyopadhyay, D., & Chakrabarti, S. (2023). Adsorptive recovery of heavy metal ions from aquatic systems using metal–organic frameworks: A perspective in the sustainable development of nanomaterials. *ChemistrySelect, 8*, e202302015. https://doi.org/10.1002/slct.202302015

Serwecińska, L. (2020). Antimicrobials and antibiotic-resistant bacteria: A risk to the environment and to public health. *Water, 12*, 3313. https://doi.org/10.3390/w12123313

Shahabi, M., Ahmadpour, A., & Raissi, H. (2024). Assessment of water purification by IRMOF-1 based on rGO as a new nanoengineered adsorbent: Insights from adsorption mechanism. *Journal of Molecular Liquids, 400*, 124485. https://doi.org/10.1016/j.molliq.2024.124485

Sharma, P., Sharma, M., Laddha, H., Gupta, R., & Agarwal, M. (2023). Non-toxic and biodegradable κ-carrageenan/ZnO hydrogel for adsorptive removal of norfloxacin: Optimization using response surface methodology. *International Journal of Biological Macromolecules, 238*, 124145. https://doi.org/10.1016/j.ijbiomac.2023.124145

Shirazian, S., Alsaab, H. O., Zare, M. H., & Yang, Q. (2025). Enhancing polysulfone membranes with UiO-66-NH2@TiO2 for humic acid removal in a PMR under visible light. *npj Clean Water, 8*, 65. https://doi.org/10.1038/s41545-025-00498-8

Sporsho, S. S., Saha, D., Khan, M. H., Rahman, M. S., Rukh, M., Islam, M. R., & Islam, M. S. (2025). Insights into adsorbent-based pharmaceutical wastewater treatment and future developments toward sustainability. *RSC Advances, 15*, 50597–50632. https://doi.org/10.1039/D5RA06445G

Stylianou, M., Christou, A., Michael, C., Agapiou, A., Papanastasiou, P., & Fatta-Kassinos, D. (2021). Adsorption and removal of seven antibiotic compounds present in water with the use of biochar derived from the pyrolysis of organic waste feedstocks. *Journal of Environmental Chemical Engineering, 9*, 105868. https://doi.org/10.1016/j.jece.2021.105868

Sultana, N., Priyadarshini, P., & Parida, K. (2025). UiO-66-NH2 and its functional nanohybrids: Unlocking photocatalytic potential for clean energy and environmental remediation. *Sustainable Energy & Fuels, 9*, 3458–3494. https://doi.org/10.1039/D5SE00150A

Sun, Y. (2025). UiO-66 metal–organic framework membranes: Structural engineering for separation applications. *Membranes, 15*, 8. https://doi.org/10.3390/membranes15010008

Sutherland, C. (2025). Exploring the state-of-the-art in metal–organic frameworks for antibiotic adsorption: A review of performance, mechanisms, and regeneration.

Environmental Toxicology and Chemistry, 44, 880–894. https://doi.org/10.1093/etojnl/vgaf009

Tai, R., Xu, W., Sui, X., Liu, X., Wang, C., & Wang, Q. (2025). Efficient adsorption and mechanism analysis of antibiotics by UiO-66-NH2/Bi2MoO6 composite materials. *Separation and Purification Technology, 360*, 130818. https://doi.org/10.1016/j.seppur.2024.130818

Tang, J., Wang, L., Qin, W., Qing, Z., Du, C., Xiao, S., & Yan, B. (2023). High reusability and adsorption capacity of acid washed calcium alginate/chitosan composite hydrogel spheres in the removal of norfloxacin. *Chemosphere, 335*, 139048. https://doi.org/10.1016/j.chemosphere.2023.139048

Tang, S., Wang, Y., He, P., Wang, Y., & Wei, G. (2024). Recent advances in metal–organic framework (MOF)-based composites for organic effluent remediation. *Materials, 17*, 2660. https://doi.org/10.3390/ma17112660

Tao, Y., Du, J., Cheng, Y., Lu, J., Min, D., & Wang, H. (2023). Advances in application of cellulose–MOF composites in aquatic environmental treatment: Remediation and regeneration. *International Journal of Molecular Sciences, 24*, 7744. https://doi.org/10.3390/ijms24097744

Teng, J., Liu, Y., Li, P., Liu, T., & Liu, X. (2025). Recyclable ZIF-8 inserted boronic acid-modified bacterial nanocellulose microspheres for improved tetracyclines removal from hoggery wastewater. *International Journal of Biological Macromolecules, 306*, 140914. https://doi.org/10.1016/j.ijbiomac.2025.140914

Tran, H. N., Lima, E. C., Juang, R. S., Bollinger, J. C., & Chao, H. P. (2021). Thermodynamic parameters of liquid–phase adsorption process calculated from different equilibrium constants related to adsorption isotherms: A comparison study. *Journal of Environmental Chemical Engineering, 9*, 106674. https://doi.org/10.1016/j.jece.2021.106674

Treskova, M., Kuhlmann, A., Freise, F., Kreienbrock, L., & Brogden, S. (2022). Occurrence of antimicrobial resistance in the environment in Germany, Austria, and Switzerland: A narrative review of existing evidence. *Antibiotics, 10*, 728. https://doi.org/10.3390/microorganisms10040728

Viltres, H., Phung, V., Gupta, N., Morera-Boado, C., Mohammadi Sheikhlar, A., Reza Rajabzadeh, A., & Srinivasan, S. (2024). Rapid and effective antibiotics elimination from water by Fe-BTB MOF: An insight into adsorption mechanism. *Journal of Molecular Liquids, 397*, 124105. https://doi.org/10.1016/j.molliq.2024.124105

Vinesh, V., Ashokkumar, M., & Neppolian, B. (2020). rGO supported self-assembly of 2D nano sheet of (g-C3N4) into rod-like nano structure and its application in sonophotocatalytic degradation of an antibiotic. *Ultrasonics Sonochemistry, 68*, 105218. https://doi.org/10.1016/j.ultsonch.2020.105218

Wang, B., Gao, C., Li, H., Zhang, Y., Jin, X., Xu, C., & Xue, W. (2023). High-efficiency degradation of norfloxacin by cathodic micro-arc plasma electrolysis: Optimization of operation parameters and investigation on kinetics. *Separation and Purification Technology, 319*, 124036. https://doi.org/10.1016/j.seppur.2023.124036

Wang, C. Y., Wang, C. C., Zhang, X. W., Ren, X. Y., Yu, B., Wang, P., & Fu, H. (2022). A new Eu-MOF for ratiometrically fluorescent detection toward quinolone antibiotics and selective detection toward tetracycline antibiotics. *Chinese Chemical Letters, 33*, 1353–1357. https://doi.org/10.1016/j.cclet.2021.08.095

Wang, C., Kim, J., Tang, J., Kim, M., Lim, H., Malgras, V., & Yamauchi, Y. (2020). New strategies for novel MOF-derived carbon materials based on nanoarchitectures. *Chem, 6*, 19–40. https://doi.org/10.1016/j.chempr.2019.09.005

Wang, H., Lou, X., Hu, Q., & Sun, T. (2021). Adsorption of antibiotics from water by using Chinese herbal medicine residues derived biochar: Preparation and properties studies. *Journal of Molecular Liquids, 325*, 114967. https://doi.org/10.1016/j.molliq.2020.114967

Wang, J., & Guo, X. (2020). Adsorption kinetic models: Physical meanings, applications, and solving methods. *Journal of Hazardous Materials, 390*, 122156. https://doi.org/10.1016/j.jhazmat.2020.122156

Wang, K., Wu, J., Zhu, M., Zheng, Y. Z., & Tao, X. (2020). Highly effective pH-universal removal of tetracycline hydrochloride antibiotics by UiO-66-(COOH)2/GO metal–organic framework composites. *Journal of Solid State Chemistry, 284*, 121200. https://doi.org/10.1016/j.jssc.2020.121200

Wang, K., Yao, R., Zhang, D., Peng, N., Zhao, P., Zhong, Y., & Liu, C. (2023). Tetracycline adsorption performance and mechanism using calcium hydroxide-modified biochars. *Toxics, 11*, 841. https://doi.org/10.3390/toxics11100841

Weerasundara, L., Gabriele, B., Figoli, A., Ok, Y. S., & Bundschuh, J. (2021). Hydrogels: Novel materials for contaminant removal in water—A review. *Critical Reviews in Environmental Science and Technology, 51*, 1970–2014. https://doi.org/10.1080/10643389.2020.1776055

Wei, F., Liu, H., Ren, Q., Yang, L., Qin, L., Chen, H., & Wang, S. (2023). Preparation of Zr-MOF for the removal of norfloxacin from an aqueous solution. *Inorganic Chemistry Communications, 153*, 110819. https://doi.org/10.1016/j.inoche.2023.110819

Wu, Z., Liu, W., Zhang, S., Peng, Z., Dong, Y., Huang, Z., & Liang, Y. (2022). Synthesis and evaluation of UiO-66@MIP towards norfloxacin in water. *RSC Advances, 12*, 20785–20791. https://doi.org/10.1039/D2RA02726G

Wu, Z., Shao, X., & Wang, Q. (2025). Antibiotics and antibiotic resistance genes in the environment: Dissemination, ecological risks, and remediation approaches. *Microorganisms, 13*, 1763. https://doi.org/10.3390/microorganisms13081763

Xia, J., Gao, Y., & Yu, G. (2021). Tetracycline removal from aqueous solution using zirconium-based metal-organic frameworks (Zr-MOFs) with different pore size and topology: Adsorption isotherm, kinetic and mechanism studies. *Journal of Colloid and Interface Science, 590*, 495–505. https://doi.org/10.1016/j.jcis.2021.01.046

Xiong, J., Zhang, D., Lin, H., & Chen, Y. (2020). Amphiprotic cellulose mediated graphene oxide magnetic aerogels for water remediation. *Chemical Engineering Journal, 400*, 125890. https://doi.org/10.1016/j.cej.2020.125890

Xu, X., Shi, L., Liu, Q., Zhong, J., Lu, M., Yang, L., & Guan, X. (2025). pH-resilient magnetic biochar-MOF hybrids for sustainable norfloxacin removal: Synergistic confinement and coordination mechanisms in real aquatic matrices. *Chemical Engineering Journal, 523*, 168752. https://doi.org/10.1016/j.cej.2025.168752

Yang, H., Wang, S., Liu, Y., Hu, Y., & Shen, W. (2024). ZIF-67 grows in chitosan-rGO hydrogel beads for efficient adsorption of tetracycline and norfloxacin. *Separation and Purification Technology, 330*, 125208. https://doi.org/10.1016/j.seppur.2023.125208

Yang, L., Bi, L., Tao, X., Shi, L., Liu, P., Lv, Q., & Li, J. (2024). Highly efficient removal of tetracyclines from water by a superelastic MOF-based aerogel: Mechanism quantitative analysis and dynamic adsorption. *Journal of Environmental Management, 353*, 120169. https://doi.org/10.1016/j.jenvman.2024.120169

Yao, N., Li, C., Yu, J., Xu, Q., Wei, S., Tian, Z., & Shen, J. (2020). Insight into adsorption of combined antibiotic-heavy metal contaminants on graphene oxide in water. *Separation and Purification Technology, 236*, 116278. https://doi.org/10.1016/j.seppur.2019.116278

Yongjia, Z., Islam, M. A., Rupam, T. H., Jahan, I., & Saha, B. B. (2024). Enhanced CO2 adsorption onto in situ ligand-impregnated mixed metal MOFs. *Colloids and Surfaces A: Physicochemical and Engineering Aspects, 703*, 135179. https://doi.org/10.1016/j.colsurfa.2024.135179

Yousaf, I., Haq, N. U., Batool, M., Khan, A. A., Parvez, M. A., & Arifuzzaman, M. (2026). Interface-directed design of glycidyl methacrylate-functionalized UiO-66 for thin film nanofiltration membranes in heavy metals rejection. *Scientific Reports*. https://doi.org/10.1038/s41598-026-39047-9

Yu, Z., Hai, C., Li, Y., Li, X., Sun, H., Zhou, Y., & Zeng, Y. (2025). Role of pH regulator on controlling the adsorption performance of LDHs type adsorbents toward Li+ from brines. *Desalination, 614*, 119125. https://doi.org/10.1016/j.desal.2025.119125

Yue, J., Li, C., Ji, X., Tao, Y., Lu, J., Cheng, Y., & Wang, H. (2023). Highly tough and conductive hydrogel based on defect-patched reduction graphene oxide for high-performance self-powered flexible sensing micro-system. *Chemical Engineering Journal, 466*, 143358. https://doi.org/10.1016/j.cej.2023.143358

Zhang, F., Wang, J., Tian, Y., Liu, C., Zhang, S., Cao, L., & Zhang, S. (2023). Effective removal of tetracycline antibiotics from water by magnetic functionalized biochar derived from rice waste. *Environmental Pollution, 330*, 121681. https://doi.org/10.1016/j.envpol.2023.121681

Zhang, F., Zhang, D., Ran, X., Xiao, M., Gan, L., Yang, X., & Sun, Q. (2025). Alginate-encapsulated ZIF-67 composite gel spheres for enhanced tetracycline removal and fixed-bed application. *Colloids and Surfaces B: Biointerfaces, 256*, 115082. https://doi.org/10.1016/j.colsurfb.2025.115082

Zhang, H. M., Wang, Y. L., Zhu, X. F., Huang, Z. Z., Pang, D. D., Wang, K., & Zhang, J. H. (2024). Application of UiO-66 and its composites for remediation and resource

recovery of typical environmental contaminants: A review. *Rare Metals, 43*, 2498–2526. https://doi.org/10.1007/s12598-023-02591-8

Zhang, L., Yang, W., Chen, Y., & Yang, L. (2025). Removal of tetracycline from water by biochar: Mechanisms, challenges, and future perspectives. *Water, 17*, 1960. https://doi.org/10.3390/w17131960

Zhang, M., Shao, S., Li, P., & Zhou, R. (2023). Removing norfloxacin from aqueous solutions using biochar derived from waste disposable bamboo chopsticks. *Water, 15*, 4306. https://doi.org/10.3390/w15244306

Zhang, S., Ding, J., Tian, D., Su, W., Liu, C., Zhang, J., & Lu, M. (2024). Adsorption behavior and mechanism of NH2-MIL-101(Cr)@COFs@SA composite adsorbent for tetracycline removal. *Polymer, 312*, 127631. https://doi.org/10.1016/j.polymer.2024.127631

Zhang, Y., Wang, Y., Wang, K., & Xiong, X. (2025). Facile preparation of recyclable porous poly(glycidyl methacrylate) microsphere with in-situ grown UiO-66-NH2 MOF for adsorption of fluoroquinolone antibiotics. *Reactive and Functional Polymers, 212*, 106261. https://doi.org/10.1016/j.reactfunctpolym.2025.106261

Zhang, Z., Chen, Y., Hu, C., Zuo, C., Wang, P., Chen, W., & Ao, T. (2021). Efficient removal of tetracycline by a hierarchically porous ZIF-8 metal organic framework. *Environmental Research, 198*, 111254. https://doi.org/10.1016/j.envres.2021.111254

Zhao, C., Ma, J., Li, Z., Xia, H., Liu, H., & Yang, Y. (2020). Highly enhanced adsorption performance of tetracycline antibiotics on KOH-activated biochar derived from reed plants. *RSC Advances, 10*, 5066–5076. https://doi.org/10.1039/C9RA09208K

Zhao, R., Shi, X., Ma, T., Rong, H., Wang, Z., Cui, F., & Wang, C. (2021). Constructing mesoporous adsorption channels and MOF–polymer interfaces in electrospun composite fibers for effective removal of emerging organic contaminants. *ACS Applied Materials & Interfaces, 13*, 755–764. https://doi.org/10.1021/acsami.0c20404

Zhao, Y., Zheng, Y., Lei, S., Jiang, X., Zhang, Y., Zhao, J., & Gao, J. (2025). MOFs functionalized magnetic sawdust hydrochar for effective tetracycline elimination: Inherent roles of adsorption and mechanisms. *Separation and Purification Technology, 378*, 134534. https://doi.org/10.1016/j.seppur.2025.134534

Zhao, Z., Yang, Y., Yu, X., Zhang, G., Li, S., Yan, Z., & Xiao, X. (2026). Catalytic thermal decomposition of ammonium perchlorate by symmetric floral CoMg-MOF and its derived carbon composites: Higher heat release and enhanced catalytic performance. *Fuel, 403*, 136147. https://doi.org/10.1016/j.fuel.2025.136147

Zheng, A. L. T., Teo, E. Y. L., Seenivasagam, S., Yiu, P. H., Boonyuen, S., Chung, E. L. T., & Andou, Y. (2025). Recent review on porous adsorbents for water decontamination: Strategies for enhanced removal of tetracycline. *Journal of Porous Materials, 32*, 1–25. https://doi.org/10.1007/s10934-024-01699-1

Zheng, C., Wu, Q., Hu, X., Ma, J., Sun, K., Sun, Y., & Xu, B. (2024). Macro-manufacturing robust and stable metal–organic framework beads for antibiotics

removal from wastewater. *Environmental Research, 246*, 118564. https://doi.org/10.1016/j.envres.2024.118564

Zheng, M., Shao, Y., Ma, F., Li, W., & Guo, M. (2025). Adsorption of antibiotics in medical wastewater by MOF-based hydrogel composites: A comprehensive review. *Journal of Water Process Engineering, 76*, 108268. https://doi.org/10.1016/j.jwpe.2025.108268

Zheng, X., Pan, C., Zheng, S., & Guo, Y. (2024). Functionalized magnetic chitosan-based adsorbent for efficient tetracycline removal: Deep investigation of adsorption behaviors and mechanisms. *Separation and Purification Technology, 335*, 126212. https://doi.org/10.1016/j.seppur.2023.126212

Zhou, Y., Fang, F., Lv, Q., Zhang, Y., Li, X., & Li, J. (2022). Simultaneous removal of tetracycline and norfloxacin from water by iron-trimesic metal–organic frameworks. *Journal of Environmental Chemical Engineering, 10*, 107403. https://doi.org/10.1016/j.jece.2022.107403

Zhou, Y., Lan, Y., Short, M. D., Shi, J., Zhang, Q., Xu, J., & Qian, G. (2023). Effective use of sugarcane-bagasse-derived KOH-activated biochar for remediating norfloxacin-contaminated water. *Toxics, 11*, 908. https://doi.org/10.3390/toxics11110908

Zou, S. J., Chen, Y. F., Zhang, Y., Wang, X. F., You, N., & Fan, H. T. (2021). A hybrid sorbent of α-iron oxide/reduced graphene oxide: Studies for adsorptive removal of tetracycline antibiotics. *Journal of Alloys and Compounds, 863*, 158475. https://doi.org/10.1016/j.jallcom.2020.158475

Supplementary Files

This is a list of supplementary files associated with this preprint. Click to download.

- Supplementarymaterial.docx